# University of Alberta

Retrieving surface peat moisture in an Albertan bog with Radarsat-2

by

Yingxiu Chen

A thesis submitted to the Faculty of Graduate Studies and Research
in partial fulfillment of the requirements for the degree of

Master of Science
in
Forest Biology and Management

Department of Renewable Resources


Fall 2013
Edmonton, Alberta

**Abstract**

Boreal peatlands are widely considered as an important carbon sink. Peat moisture is important for controlling carbon sequestration and smouldering combustion. Retrieving surface moisture is of great interest for carbon budget modelling and fire management in peatlands.

To monitor at a large scale, Radarsat-2 was used to retrieve surface (0-5 cm) peat moisture in an Albertan ombrotrophic bog. Oven-dried peat cores, FDR probes (Theta probe) and TDR probes (CS616) were used for the field sampling of volumetric moisture content (VMC). Non-polarimetric analysis was performed to extract backscattering coefficients from Radarsat-2 images in NEST. The model was built with multiple linear regression in SAS. This approach shows promise for the burned plots (concordance correlation coefficient ρ: 0.435; accuracy: 0.997), followed by all sampled plots (ρ: -0.254; accuracy: 0.962) and unburned plots (ρ: 0.153; accuracy: 0.821).

**ACKNOWLEDGEMENTS**

I would like to thank Alberta Sustainable Resource Development for funding and Canadian Space Agency (CSA), MacDonald Dettwiler and Associates (MDA) and Natural Resources Canada (NRCan) for providing Radarsat-2 images.

Dr. Mike Flannigan, as my supervisor, is providing supportive feedback all through my Master project. He helped me rebuild my confidence and interests in scientific research. His timely feedbacks and guidance clarify my academic and life perplexities. His patience, kindness, openness and toleration greatly influence my way of thinking and behavior. Without his support and guidance, I couldn't have the opportunity and the strengths to finish my Master here.

I would like to thank Dr. Dan Thompson with help in setting up the weather station, species identification, field sampling and data analysis and other guidance. His timely and helpful feedback is always highly appreciated.

I would like to thank Dr. John Gamon for his valuable advice. His careful and thought-provoking questions help me think deeper about my project.

I would also like to thank Ms. Chelene Krezek-Hanes for technical support in radar image ordering and processing. I would also like to thank Mr. Alec Casey and Mr. Iman Entezari for technical support in radar image processing.

Thanks Stephanie Koroscil, Karen Blouin, Dan Thompson, Oleg Melnik, Jacqueline Dewar and Thomas Fleming for their help with field sampling. Thanks Ginny Marshall for proofreading.

I would like to thank Mr. Ian Paine for recovering my thesis. My laptop crashed in January with my thesis inside and I didn't have a backup copy then. Thanks to Mr. Ian's efforts, my thesis was back! I can't describe how grateful I am!

I would also thank my parents and my sister, especially my mother. Her perseverance and optimism greatly shape who I am. I would also thank all my friends who care and help me. Without their encouragement and advice, I couldn't have the courage and strengths to finish writing this thesis.

**TABLE OF CONTENTS**

LIST OF TABLES

LIST OF FIGURES

# INTRODUCTION

Peat is a type of histosol that contains less than 25% inorganic material on a dry weight basis (Andrejko et al. 1983.; Zoltai et al. 1998). In Canada, a minimum thickness of 40 cm peat is required to be classified as peatlands (National Wetlands Working Group 1988). Approximately 14% or $10^6$ $km^2$ of the total surface land area in Canada is peatlands, as shown in Figure 1 (National Wetlands Working Group 1988; Zoltai et al. 1998). In Alberta, it is about 20% or $1.3 \times 10^5$ $km^2$ (National Wetlands Working Group 1988), as shown in Figure 2.

Boreal peatlands are widely considered as an important carbon sink (Turetsky et al. 2002; Turunen et al. 2002), containing about 455 Pg (1 Pg=$10^{15}$ g) carbon or nearly a third of the world's total soil carbon reservoir (Gorham 1991). However, due to global warming, it is estimated that as much as 100 Pg carbon may be lost by 2100 in peatlands (Davidson and Janssens 2006). Carbon storage is driven by the movement of water in peats (Holden 2005) and the rate of sequestration and release of greenhouse gases such as $CO_2$ and $CH_4$ is controlled in part by peat moisture (Moore and Knowles 1989; Dise 1993). Because greenhouse gases release is largely regulated by peat moisture, retrieving surface moisture in peatlands is of paramount importance for mitigating global climate and carbon sequestration (Belyea and Malmer 2004; Holden 2005).


Figure 1. Boreal peatlands of Canada (National Wetlands Working Group 1988). The red star shows the study area.

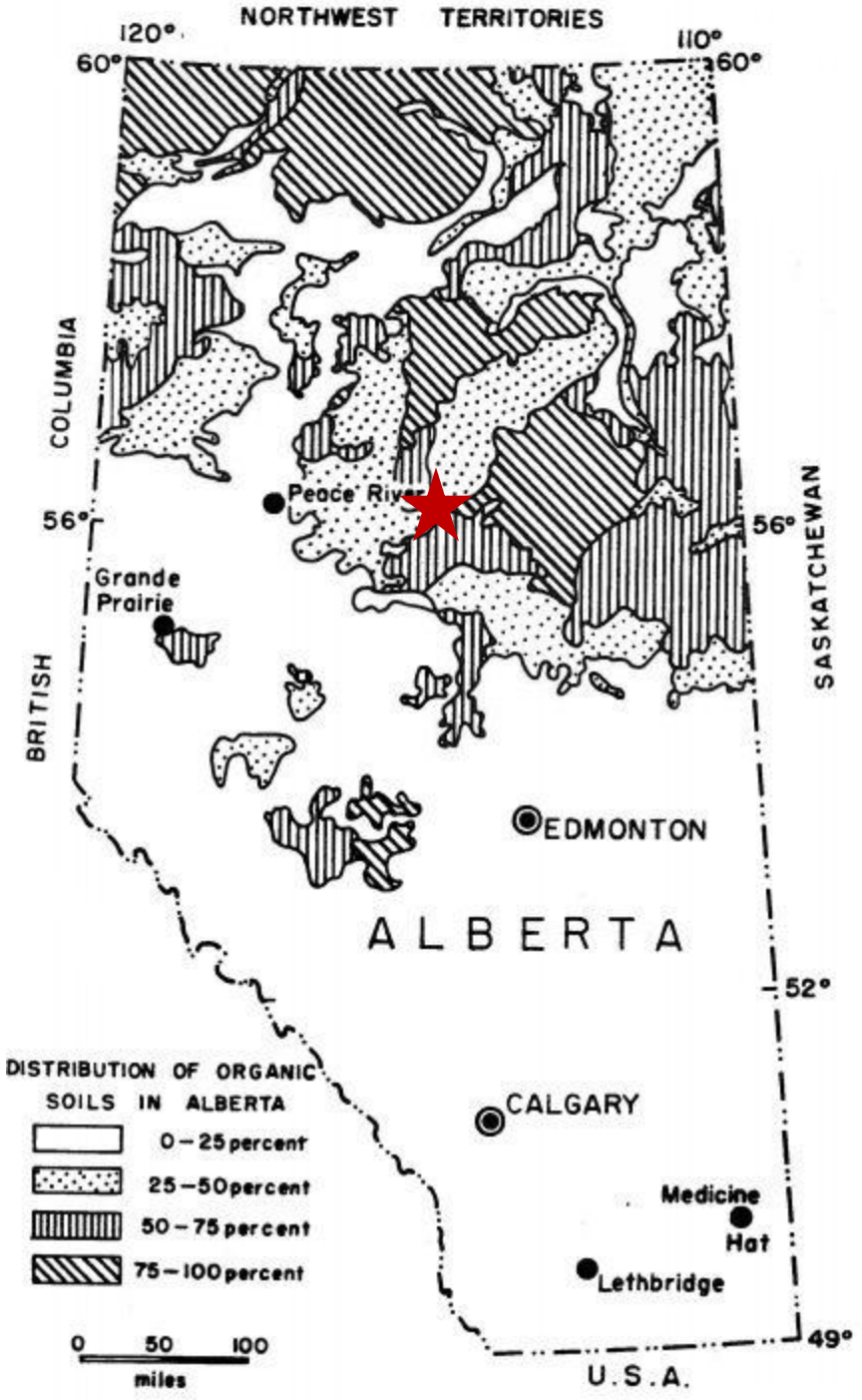


Figure 2. Peat distribution in Alberta (Alberta Energy and Utilities Board and Alberta Geological Survey 1967). The red star shows the study area.

## Peatland fires

Although peatland fires would seem very unlikely to take place at first glance, occasionally they do happen (Watts and Kobziar 2012). Peatlands fires usually take the form of smouldering combustion. Smouldering is a "slow, low-temperature, flameless form of combustion" (Ohlemiller 2002), where oxidation reaction occurs in the solid surface of the fuel (peats in this case) (Rein 2009). Once ignited, peats can smoulder for months or even years, spreading vertically down to several meters and laterally far away underground (Hadden et al. 2013; Watts and Kobziar 2013). This characteristic is the main reason that peatland fires are so difficult to suppress (Flannigan et al. 2009a). Thus far, very few modern techniques have been proved to be effective in suppressing such underground peat fires (Watts and Kobziar 2013).

Primarily based on hydrological and chemical properties, peatlands can be further classified as either ombrotrophic bogs (ombrogensus systems influenced only by precipitation) or minerotrophic fens (geogenous systems influenced by ground water) (Vitt et al. 1994; Vitt et al. 1995; Flannigan et al. 2009a). Based on the peatland type in this study area, the focus in this thesis is non-permafrost continental bogs.

Due to the thickness and high carbon density of peats (Schimel and Baker 2002), wild peatland fires can emit extremely high amounts of carbon. Consequently, large carbon loss due to peat fires greatly reduces carbon sequestration in peatlands (Turetsky et al. 2002; Turetsky and Louis 2006). On long-term average, it is estimated that ~100 $km^2$ non-permafrost continental bogs in Alberta burn annually, based on Table 5 in (Zoltai et al. 1998). Also, it is estimated that about 5~7 Tg (1 Tg=$10^{12}$ g) carbon per year are being released to the atmosphere as a consequence of the effects of western Canadian peat fires under current disturbance regimes (Turetsky et al. 2002). In addition to greenhouse gases, peat fires will also release irritating gases and particles such as $PM_{2.5}$ (particulate matter with an average size of 2.5 microns or smaller), sulphur, nitrous oxides and mercury, posing health threats for vulnerable populations such as the elderly, children and asthmatics. (Byron and Shepherd 2009; Flannigan et al. 2009a; Rappold et al. 2011; Watts and Kobziar 2013).

In the face of global warming, fire activity (area burned, fire season and fire occurrence) will continue to increase (Flannigan et al. 2009b), leading to increased

burning in boreal and subarctic peatlands (Turetsky et al. 2004). With more peat fires due to global warming, it is very likely that more holdover fires would take place, which can remain dormant in the winter and flare up in the coming spring (Flannigan et al. 2009a). Such holdover fires with little heat and flame are not easy for visual detection and hence can be quite dangerous (Niederleitner 1976). One of the critical factors that determines whether smouldering can or cannot propagate is peat moisture content (Frandsen 1987). To be specific, surface peat moisture, together with bulk density and inorganic content, influences this process by its impact on heat of ignition and the released heat that will be available for propagating the combustion front (Benscoter et al. 2011). Hence, retrieving surface moisture in peatlands is of great interest for fire hazard assessment in peatlands.

## SAR background

Although peat moisture content is a vital parameter, it is still not widely and routinely incorporated into environmental models (Barrett et al. 2009). This is primarily due to its inherent spatial and temporal variability and the drawbacks of conventional field sampling methods (Engman and Chauhan 1995; Biftu and Gan 1999). Here the conventional methods refer to the oven-dried gravimetric method, theta probes and Time Domain Reflectometer (TDR). These conventional approaches are time-consuming, point- based and site -specific.

By contrast, remote sensing offers a time- and economic- efficient way to overcome the shortcomings of conventional methods (Ramsey 1995). With remote sensing, it is economically feasible for regional or global retrieving of surface soil moisture on a frequent basis (Moran et al. 2000). Among the electromagnetic spectrum from radio to visible spectrum, Synthetic Aperture Radar (SAR) images from the microwave spectrum hold greatest promise for retrieving soil moisture (Jackson 1993; Engman and Chauhan 1995; Gala et al. 2011). Compared with optical sensors such as Landsat, one particular feature about SAR is that it can acquire images under almost all weather conditions because of its long wavelength (in the range of decimeter) and both day and night because of its active sensor (Jackson 1993). Also, because of its active sensor, usually SAR has a very high spatial resolution compared with infrared sensors such as Moderate Resolution Imaging Spectroradiometer (MODIS). Finally, SAR can monitor underlying surfaces features such as surface soil moisture content (Engman and Chauhan 1995)

because SAR can "see through" vegetation with such long wavelength (Schmugge et al. 2002).

In real life application, SARs are usually either air-borne (aircraft/shuttle) or space-borne (satellite). The formidably high price and limited coverage of air-borne SAR images often preclude a regular and frequent access to such data. By comparison, space-borne SARs offer a more economical choice. In summary, all the previously discussed technical features of space-borne SARs offer researchers enormous opportunities for retrieving surface peat moisture.

Since 1990s, numerous researchers all over the world have been studying the application of SAR to retrieve soil moisture, e.g. (Kasischke et al. 1995; Biftu and Gan 1999; Baghdadi et al. 2002a; Sass and Creed 2008; Gherboudj et al. 2011). Basically, the rationale of how SAR works is by taking advantage of the large contrast in dielectric constant of water (as much as 80) and dry soil (less than 5) (Schmugge et al. 1974). Changing moisture content (wetness) of soil will dramatically affect soil dielectric constant. At the same time, soil moisture is directly proportional to its dielectric constant (see Figure 3.) (Dobson et al. 1985; Brisco et al. 1992). Consequently, this sensitivity to water content enables SAR to detect surface soil moisture content (Dubois et al. 1995; Brisco and Brown 1998).

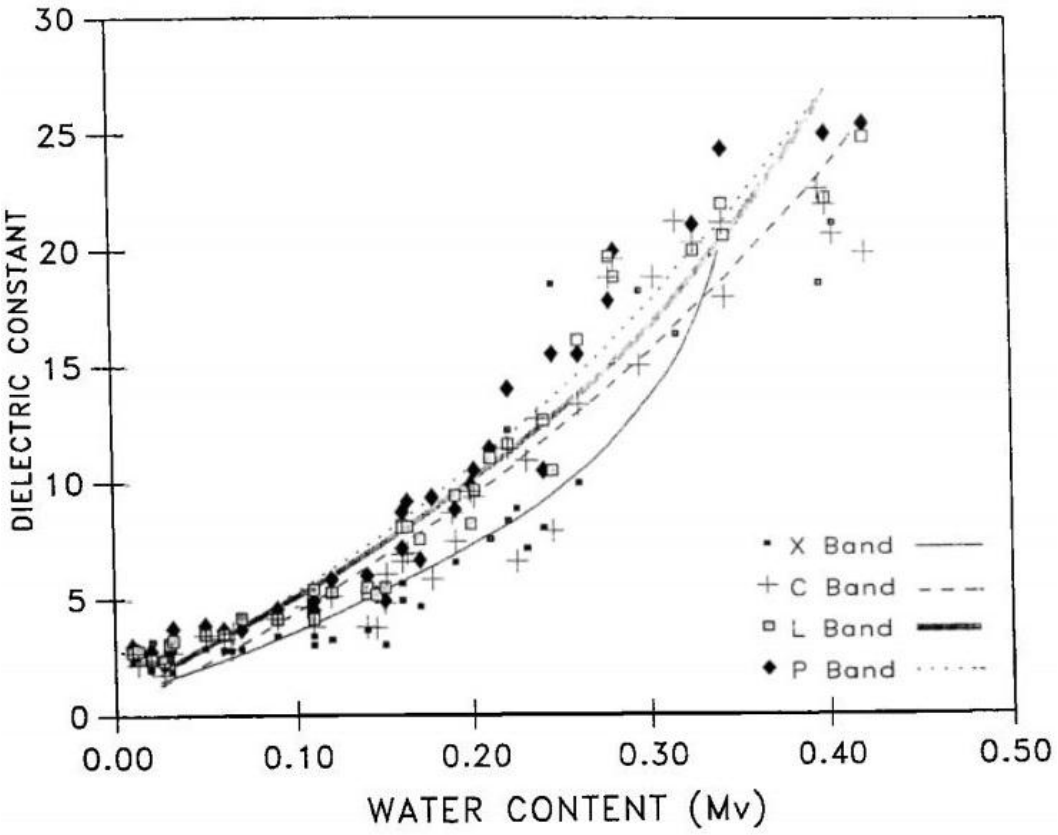


Figure 3. Relationship between dielectric constant and water content for 4 bands, after (Brisco et al. 1992). X band wavelength: 3.75- 2.50 cm; C band wavelength: 7.5-3.75 cm; L- band wavelength: 30-15 cm; P band wavelength: 30- 100 cm.

The most commonly measured radar signal is radar reflectivity. This reflectivity is named as backscattering coefficient (Ulaby et al. 1981), which is also known as the normalized radar cross-section ($\sigma^\circ$). The unit of backscattering coefficient is usually intensity or decibels (dB)[1]. This parameter measures the average reflective strength of a distributed target with respect to a unit plot on the horizontal ground plane (Larter 2010). A schematic is presented in Figure 4. to demonstrate a general relationship between backscattering coefficient and soil moisture content over bare land surfaces (Sass and Creed 2008).

[1] The conversion between intensity and dB is $dB = 10*\log_{10}(\text{intensity})$.

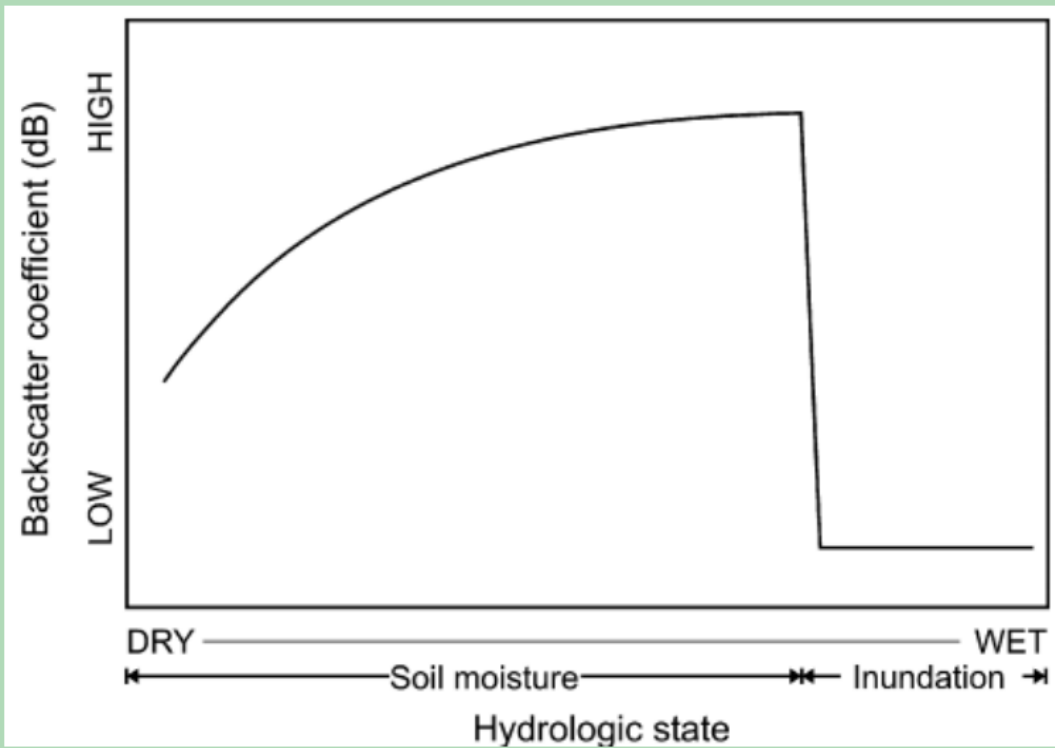


Figure 4. Schematic response backscatter to soil moisture change, after (Sass and Creed 2008).

As shown in Figure 4, there are two different stages of scattering mechanisms as soil moisture content increases: the first stage is before soil saturation and the second is after soil saturation. Before saturation, the relationship is mainly due to the large contrast in dielectric constant of water (as much as 80) and dry soil (less than 5). The relationship is non-linear because the backscattering coefficient reaches signal saturation when the soil moisture content is high (Kasischke et al. 1995; Sass and Creed 2008). The second stage is after soil saturation. At this stage, the scattering mechanism is specular reflection. Specular reflection indicates that the majority of the incoming energy is reflected away by the standing water from the sensor. Hence, little or no energy can be recorded back to the SAR. As a result, the SAR images of smooth water bodies appear dark.

Figure 4 is only an ideal diagram showing a general trend. In addition to surface soil moisture content, backscattering coefficient is also influenced by sensor configuration parameters (wavelength, polarization, and incidence angle). In addition, other surface features such as surface roughness (spatial scales to a broader sense) and vegetation are also very important.

**Wavelength, polarization, and incidence angle**

The most commonly used space-borne SARs for soil moisture estimation come at C band (~5cm) and L band (~20cm) (Lakhankar et al. 2009). The penetration depth is typically on the order of tenths of the wavelength up to half the wavelength (Ulaby et al. 1996; Koyama et al. 2010; Koyama 2012). So for retrieving surface peat moisture, usually the top 5 cm layer is sampled to correspond to the penetration depth.

C-band can "see through" up to around 20 tons/ha or 2000g/$m^2$ biomass (Imhoff 1995). Since it is estimated that the mean biomass is 619 g/$m^2$ for the tree layer and 258 g/$m^2$ for the shrub layer in non-permafrost bogs in Alberta (Campbell et al. 2000), it is suitable to use C-band for this research to estimate the surface peat moisture in an Albertan bog. Though L band may be a better candidate, such images are not available in this research. Though longer band such as L band can penetrate deeper and work better in vegetated areas than C band, currently no space-borne SARs come in L-band. ALOS-2/PALSAR-2, operating at L band, is under construction now.

Among all launched space-borne C-band SARs, Radarsat-2 is especially versatile—it offers various beam modes, providing single polarization (HH, HV, VH or VV), dual polarization (HH + HV or VV + VH) and quad polarization (HH + HV + VV + VH) images (see Figure 5). Here, polarization refers to the direction of the electric field of the electromagnetic wave transmitted or received by a radar antenna (Ulaby et al. 1996). It can come in either horizontal (H) or vertical (V) polarization. Co-polarization in this thesis is referred to as HH, VV and their dB forms while cross-polarization is HV, VH and their dB forms. Other features of Radarsat-2 are multi-incidence angles and multi-spatial resolutions. Also, Radarsat-2 has a very stable performance with a radiometric error less than 1 dB (MacDonald Dettwiler Associates Ltd 2011).

The optimal incidence angle for soil moisture retrieval with SAR is low incidence angle because the influence of surface roughness and vegetation is minimized (Ulaby et al. 1986). Also low incidence angle yields low error (Bryant et al. 2007).

In this research, the beam mode FQ3--Fine Quad-polarization (HH+VV+HV+VH) was chosen based on its quad polarization, low incidence angle (21.10 degrees) and high resolution (pixel size ~ 5m). With this beam mode, the revisit period or temporal resolution is 24 days.

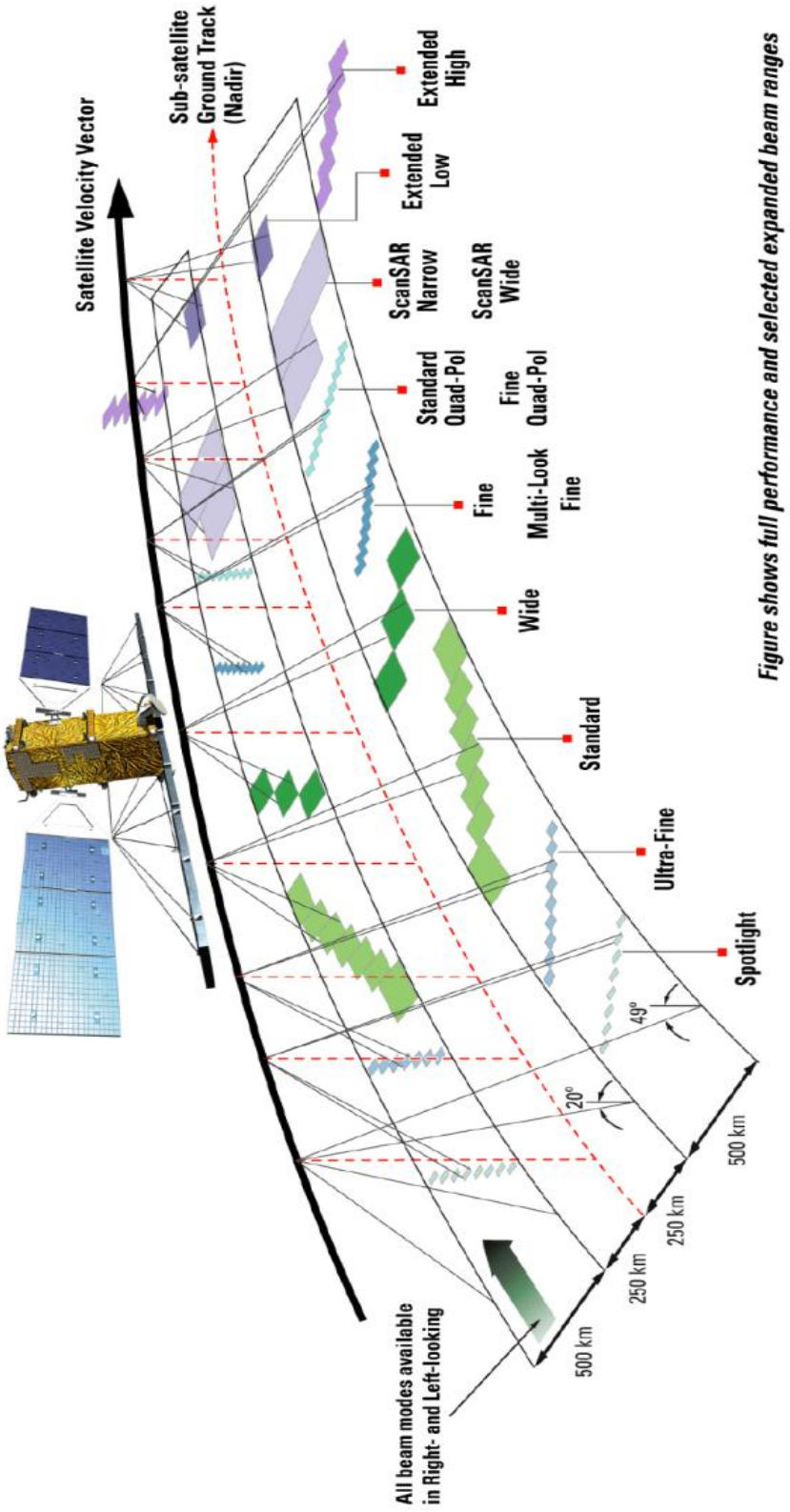


Figure 5. Radarsat-2 beam modes, after (MacDonald Dettwiler Associates Ltd 2009).

## Peatland spatial scales

As mentioned above, surface roughness (spatial scales to a broader sense) is an important factor influencing backscattering coefficient. Here three spatial scales are introduced: fine scales in the range of centimeters (surface roughness), meso-fine scales in the range of a few meters (hummocks and hollows) and macro scales in the range of several hundred meters (homogeneity of backscattering coefficient).

### Fine scales

The very fine spatial scales in peatland is surface roughness. Surface roughness is generally parameterized by Root Mean Square Height ($h_{rms}$), the Correlation Length (Lc) and an Autocorrelation Function (ACF) (Fung et al. 1992; Lievens et al. 2009; Merzouki et al. 2010). Lc can be derived from $h_{rms}$ empirically (Baghdadi et al. 2002b), semi-empirically (Baghdadi et al. 2004), and theoretically (Rahman et al. 2007). ACF is often assumed to be Gaussian or exponential (Fung et al. 1992; Tansey and Millington 1998). Hence, it is plausible to characterize surface roughness with only one measurement of $h_{rms}$ (Bryant et al. 2007).

However, despite numerous researchers' great efforts for years, it is still unsatisfactory to parameterize surface roughness ($h_{rms}$, Lc) for soil moisture retrieval (Lievens et al. 2011). In fact, it is believed that the main source of error in soil moisture retrieval comes from a failure to quantify roughness parameters (Verhoest et al. 2008). This may be due to four possible reasons: 1. Biases introduced by measuring instruments (the laser scanner or the pin meter); 2. Inadequate number of observations of $h_{rms}$; 3. Truncation error of transect length (Mattia et al. 2003; Bryant et al. 2007); 4. An inadequacy/inaccuracy of the single scale assumption in the scattering models (Davidson et al. 2000). Self-affine fractal models, rather than the single scale assumption adopted in the current scattering models, better describes natural surfaces (Shepard and Campbell 1999). Due to the complexities in field sampling and unsatisfactory results in literature, surface roughness was not sampled in this research.

However, it is believed that the influence of surface roughness will not cause a systematic bias in retrieving surface peat moisture. This is because, first of all, low incidence angle is selected to minimize the influence of surface roughness; secondly, the contribution of surface roughness to backscattering coefficient is already accounted in the

model developed in this research. When building the model to retrieve surface moisture, cross polarization and VV/VH are incorporated to account for the influence of surface roughness and to improve accuracy (Oh 2004).

**Mesoscales**

The meso-fine scale of surface roughness in peatland is its microtopographical features (hummocks and hollows). Hummocks are small, elongated mounds randomly or systematically separated by flatter, wetter depressions or "hollows" (Hogg 1993; Nungesser 2003). The vegetation in peatlands is dominated by *Sphagnum spp*., especially *S. fuscum* (Damman 1977; Moore 1989).

*Sphagnum* builds and maintains the hummock-hollow microtopography (Andrus et al. 1983; Rydin 1993). For example, *S. fuscum* is found primarily in hummocks and *S. angustifolium* and *S. magellanicum* in hollows. Although all *Sphagnum* species have the potential to survive or even flourish in the hollows (Rydin 1993), *S. fuscum* is excluded from the hollows. This is probably because hollow species such as *S. angustifolium* have a faster growth rate than hummock species such as *S. fuscum*. Consequently, in the long term, *S. angustifolium* outcompetes and excludes *S. fuscum* from hollows (Rydin 1986; Rydin 1993; Benscoter and Vitt 2008).

The upper bound of hummocks is restricted by the species' water retention ability (Benscoter and Vitt 2008). Hummock species have higher water retention ability than hollow species (Rydin 1993; Nungesser 2003). Consequently, hummock species are less likely to burn and less severely desiccated than hollow species during droughts (Rydin et al. 2006). Also because of the difference in water retention ability, hollow species can burn to a much higher degree compared with hummock species (Benscoter et al. 2005). As a matter of fact, it is estimated that almost twice as much carbon is lost from hollow combustion than from hummocks (Benscoter and Wieder 2003). Consequently, microtopography plays an important role in peatlands' vulnerability to wildfire and carbon lost (Thompson and Waddington 2013). A major factor influencing carbon lost in peatland fires is the difference of peat moisture (or fuel moisture in fire science) between hummocks and hollows (Wein and Bliss 1973; Benscoter and Wieder 2003; Benscoter et al. 2011; Waddington et al. 2012). In this research, the microtopographical features are reflected in the weighted average Volumetric Moisture Content (VMC).

### Macroscales

The macroscale of surface roughness generally refers to the topography such as ridge with sloping sides. However, in peatland, due to its flat landscape, the influence of such scale is estimated to be minimal, *c.f.* Figure 16. In addition, all Radarsat-2 images were orthorectified with Digital Elevation Model (DEM) to further correct for the influence of topography.

In this research, the macroscale refers to how homogenous the backscattering coefficient is. Generally speaking, the larger the area is averaged, the more homogenous the backscattering coefficient becomes. In order to investigate at what scale Radarsat-2 works best for retrieving surface peat moisture, eight scales of averaging are investigated in this research: 25m*25m, 50m*50m, 75m*75m, 100m*100m, 125m*125m, 150m*150m, 175m*175m, and 200m*200m.

## Vegetation

Another important factor that influences backscattering coefficient is vegetation. Though C band can "see through" the vegetation (tree layer and shrub layer) in this research site, the presence of vegetation complicates the moisture retrieval process: the microwave emitted by SAR now first needs to penetrate and interact with the vegetation layer and then interact with the underlying surface (Hajnsek et al. 2009).

In order to tease out the influence of vegetation, target decomposition theory may be applied. This theory enables researchers to represent the average scattering mechanism as the sum of independent physical mechanisms for each component (Touzi et al. 2004). Generally speaking, 5 main scattering mechanisms can be identified for vegetated natural surfaces, as shown in Figure 6. With target decomposition theory, the main source of scattering mechanisms can be identified.

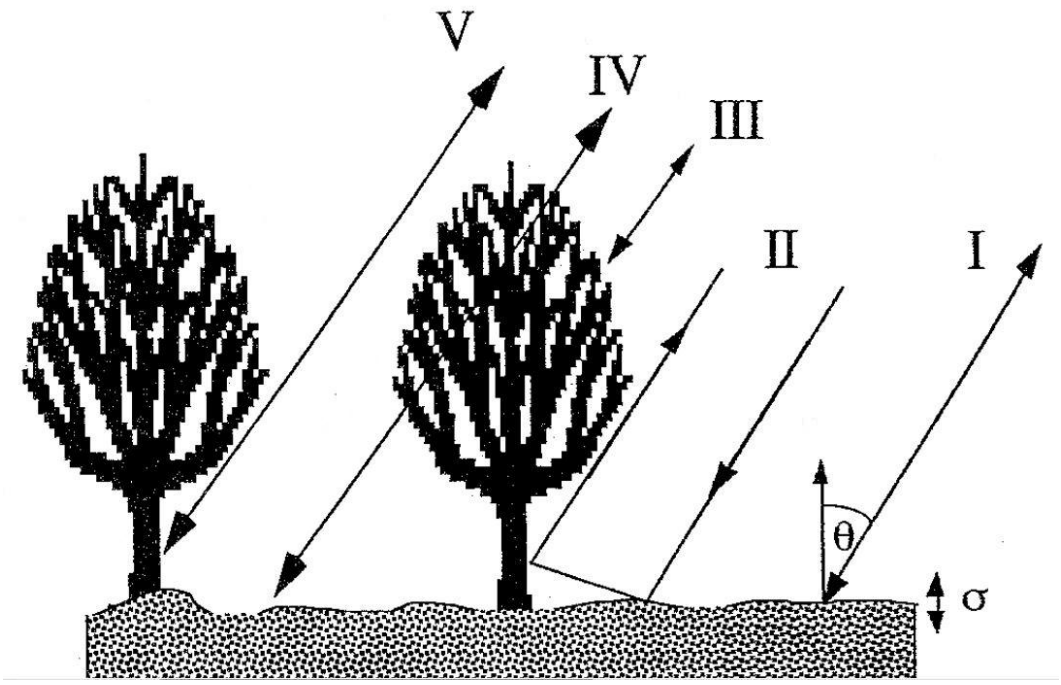


Figure 6. Schematic diagram showing the main scattering mechanisms in forest, after (Cloude and Pottier 1996), where I) Backscattering directly from the surface; II) Dihedral scattering or low-order multiple scattering; III) Volumetric backscatter from a non-penetrable layer of discrete scatters; IV) Surface scattering after propagation through the canopy, as occurs in the use of L-band radar for penetration of vegetation cover; V) Single scattering from anisotropic structures such as tree trunks.

In order to quantify the influence of vegetation, field sampling on vegetation should be carried out. Vegetation parameters are needed such as canopy height, canopy moisture content, diameter at breast height, etc. Due to constraints of manpower and time, no field sampling of vegetation was done. Though it is possible to estimate those vegetation parameters from optical images, as shown in (Lievens and Verhoest 2011), this approach is not feasible at current stage.

To further integrate these vegetation parameters into the scattering models, usually Water Cloud Model (WCM) developed in (Attema and Ulaby 1978) is used. WCM is semi-empirical model and has the feature of simplicity. But even with this relatively simple model, it still needs to be calibrated with a large dataset of both SAR signals and field measurements (Sano et al. 1998; Bindlish and Barros 2001; Moran et al. 2002; Sikdar et al. 2005; Gherboudj et al. 2011; Lievens and Verhoest 2011).

After target decomposition and field sampling on vegetation, several scattering models can be applied for surface moisture retrieval. Integral Equation Method (IEM) developed in (Fung et al. 1992; Fung 1994; Fung et al. 1996) is the most widely used scattering model (Thoma et al. 2004). Due to its complexity, the original form of IEM is rarely used. Instead, approximate solutions are often adopted to inverse IEM (Chin-Yuan et al. 1997). Usually approximate solutions require iterative techniques such as Artificial Neural Network (ANN) (Baghdadi et al. 2002a; Paloscia et al. 2008). ANN method is a good balance between accuracy (mean error ~9%) and computational time but ANN relies heavily on the training dataset (Paloscia et al. 2008). Because of the complexity of IEM and ANN and the constraints of time and resources, such methods were not adopted in this research.

### Canadian Forest Fire Danger Rating System

In the current Canadian Forest Fire Danger Rating System (CFFDRS), Fire Weather Index (FWI) is widely used to predict fire danger indexes in Canadian boreal forests (Van Wagner 1987). FWI is made of three symbolic Fuel Moisture Codes and two Fire Behavior Indices, as shown in Figure 7. These three Fuel Moisture Codes are Fine Fuel Moisture Code (FFMC), Duff Moisture Code (DMC) and Drought Code (DC). FFMC refers to the moisture of the top 1~2 cm layer of fine surface litter; DMC refers to the moisture of the 2~10 cm layer of loosely compacted, decomposing organic matter; and DC refers to the moisture of the 10~20 cm deep layer of compact organic matter (Van Wagner 1987).

Although these moisture codes have enjoyed success in boreal forests for quite a long time, they may not be suitable for fire management in peatlands. One reason is that boreal peatlands are very different from forests. All these moisture codes were developed from forests. To illustrate, FFMC was developed from eastern pine needles; DMC was from red pine and jack pine forests; and DC was from balsam fir and black spruce forests (Van Wagner 1987). All these prototypal trees are very different from peat mosses. Another reason is that none of these moisture codes take the important factor--solar radiation into account, as we can see from Figure 7. Thus far, no moisture code has been developed specifically for the peatlands (Waddington et al. 2012).

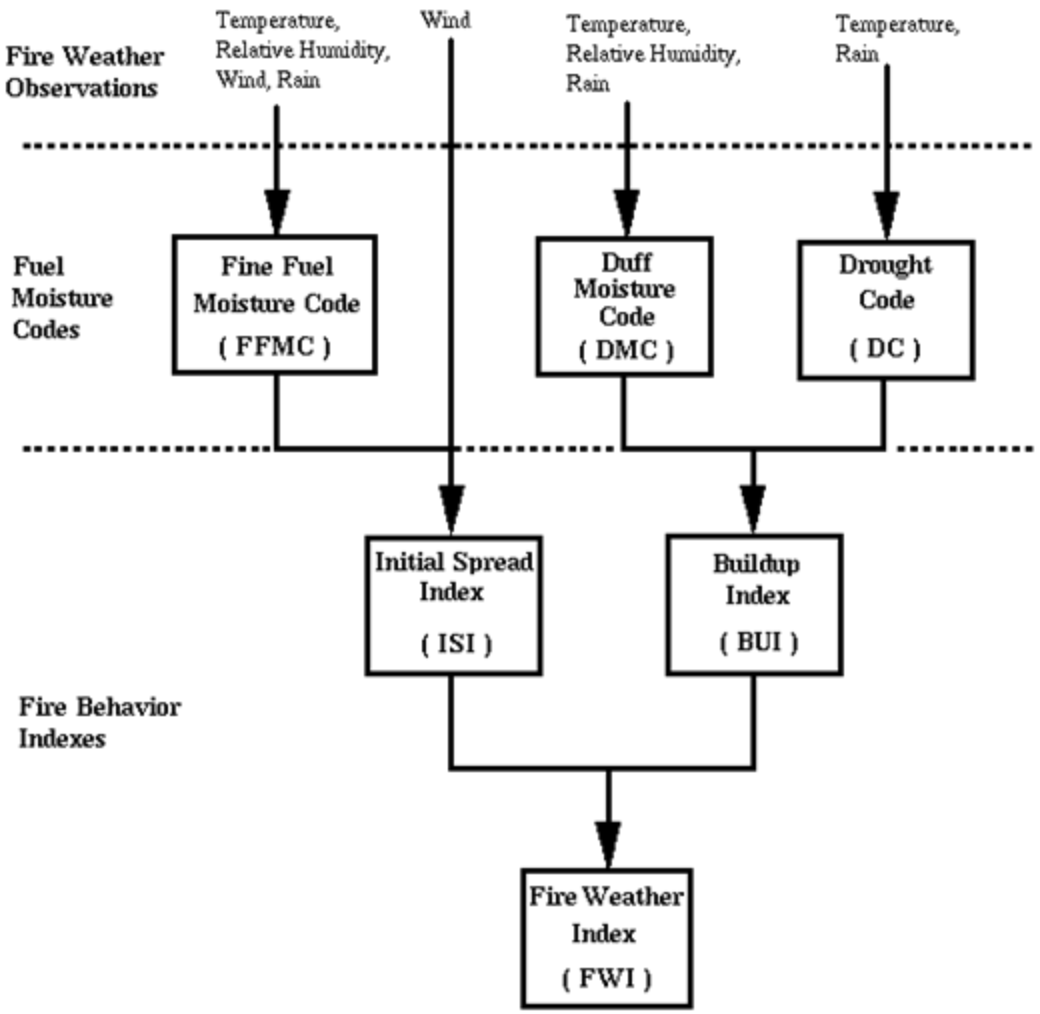


Figure 7. Structure of the FWI System (Canadian Forest Service 2013).

## Research objectives

The primary objective of this thesis is to use Radarsat-2 to retrieve surface (0-5 cm deep) peat moisture content in an Albertan ombrotrophic bog (latitude 56.36~56.37 °, longitude -115.26~ -115.29 °). The top 5 cm peat is chosen because this depth is what C-band can penetrate. So in order to correspond with the Radarsat-2 penetration depth, all field sampling methods (peat cores, theta probes and TDRs) are set to measure the moisture content of the top 5 cm peat. In addition, this top 5 cm layer is of great ecological/environmental interest because it is critical in initializing the surface fire.

In this research, the differences of both spatial and temporal variations between burned and unburned plots are examined. New conceptual models for peat moisture are proposed for future fire hazard warning system in boreal peatlands since the current CFFDRS focuses mainly on the forests. In addition, it is anticipated that this research could be helpful in refining the peatland carbon budget modeling since surface moisture controls the rate of sequestration and release of greenhouse gases (Moore and Knowles 1989; Dise 1993).

# METHODS

## Study area

This research was conducted in a non-permafrost continental ombrotrophic bog near Red Earth Creek, northern central Alberta (latitude 56.36~56.37 °, longitude -115.26~ -115.29 °). It is within the Boreal Plain ecozone, which is typified by cold winters and moderately warm summers (Hare and Thomas 1979). .

The nearest weather station is in Red Earth (Latitude: 56°40' N, Longitude: 115°7' W, Elevation 610 m), which is about 20 km from the centre of the study area. Based on the 1961–1990 climate normals in Red Earth (data source: (Environment Canada 2012)), the daily minimum temperature, daily average temperature, daily maximum temperature and precipitation are shown in Figure 8. Here, only July, August and September are shown because the field campaign was carried out on July 10 (0710), August 3 (0803), August 27 (0827), and September 20 (0920), 2012.

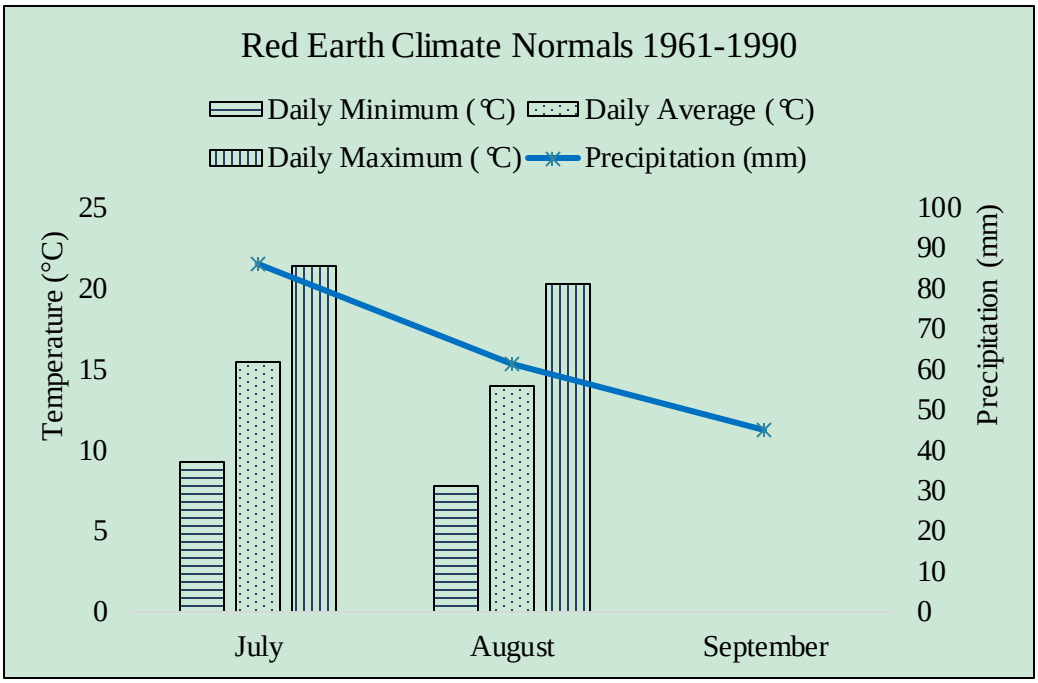


Figure 8. 1960-1990 climate normals in Red Earth. No data is available for September.

Due to a lack of data in September in Red Earth weather station, the climate normal of another nearby weather station--Slave Lake, is also given. The Slave Lake weather station (Latitude: 55°18'00" N, Longitude: 114°47'00" W, Elevation: 580.60 m) is about 150 km from the centre of the study area. Based on the 1971-2000 climate normals in Slave Lake (data source:(Environment Canada 2013)), the daily minimum temperature, daily average temperature, daily maximum temperature, soil temperature at 5 cm depth (both morning and afternoon observations) and precipitation (rainfall plus snowfall) are shown in Figure 9. Again, only July, August and September are shown because the field campaigns were carried out during these three months.

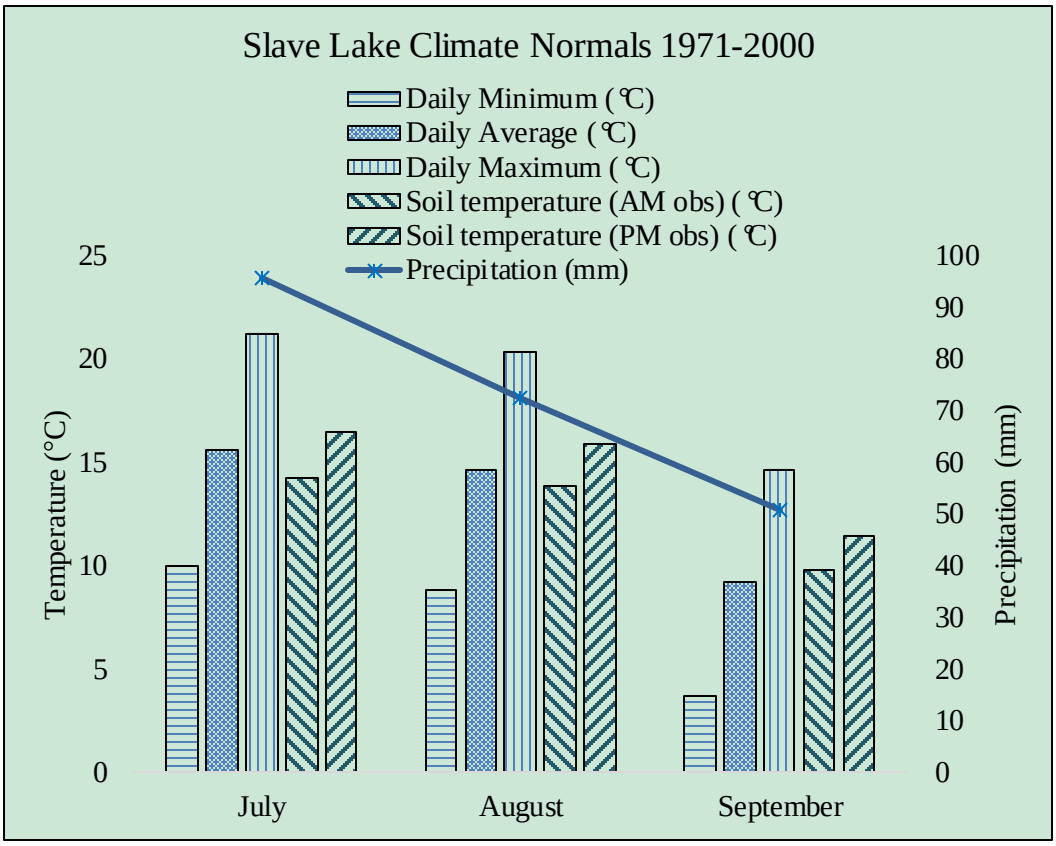


Figure 9. 1971-2000 climate normals in Slave Lake.

This study area is 600m*1600m. The site is further divided into 24 plots. Each plot is 200m*200m and is numbered as shown in Figure 14. The bryophyta in this site are mainly moss. The dominate moss species is *Sphagnum fuscum*. Other moss species include *Sphagnum angustifolium, Sphagnum magellanicum* etc. Lichens are also common in this study area and dominant in the burned plots, *c.f.* Figure 17, as also observed by (Damman 1977). As for vascular plants, there are herbaceous monocots (cotton sedges *Eriophorum*), and a range of dwarf ericaceous shrubs such as *Calluna, Erica, Ledum,* and *Chamaedaphne* (Moore 1989). Some plots are treed with black spruce (*Picea mariana*) and tamarack (*Larix laricina*) or treeless, *c.f.* Figure 16 and Figure 18.

**Weather station**

A weather station was set up on the border of Plot 1 and 4 on June 20, 2012, as indicated by a red star in Figure 14. This weather station recorded air temperature (Figure 10), Relative Humidity (RH), wind speed and direction, precipitation, and solar radiation.

The total rainfall for this sampling season (from June 21, 2012 to September 20, 2012) is 244.4mm. With these weather variables, evapotranspiration was calculated based on the Penman-Monteith equation. The assumptions for the Penman-Monteith equation are one-dimensional upwards fluxes; a Leaf Area Index (LAI) of 1.5 based on (Sonnentag et al. 2007); and a canopy height of one meter based on field observation. Seasonal trends of evapotranspiration and rain is shown in Figure 11.The total evapotranspiration for this sampling season is -742.3 mm with a median of -8.6 mm/day, with the default surface resistance at zero and with a standard aerodynamic resistance for Penman-Monteith equation. Negative evapotranspiration indicates water losses to the atmosphere. A typical diurnal trend of evapotranspiration dynamics is shown in Figure 12 for August 27, 2012.

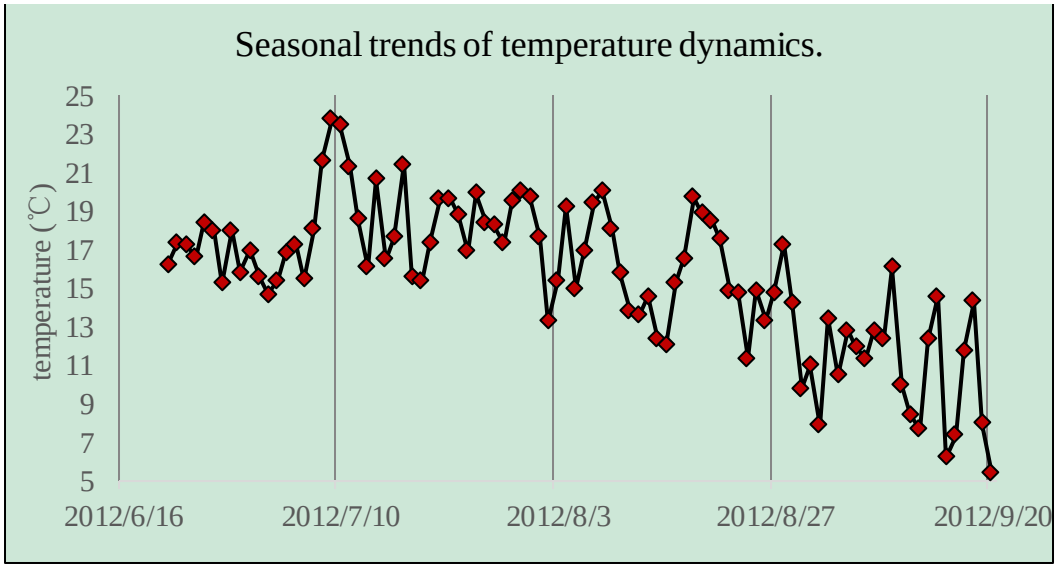


Figure 10.Seasonal trends of temperature dynamics. All dates were 24-hour average temperature except for 0920, which was the average from 0 am to 3 pm, due to the end of this experiment.

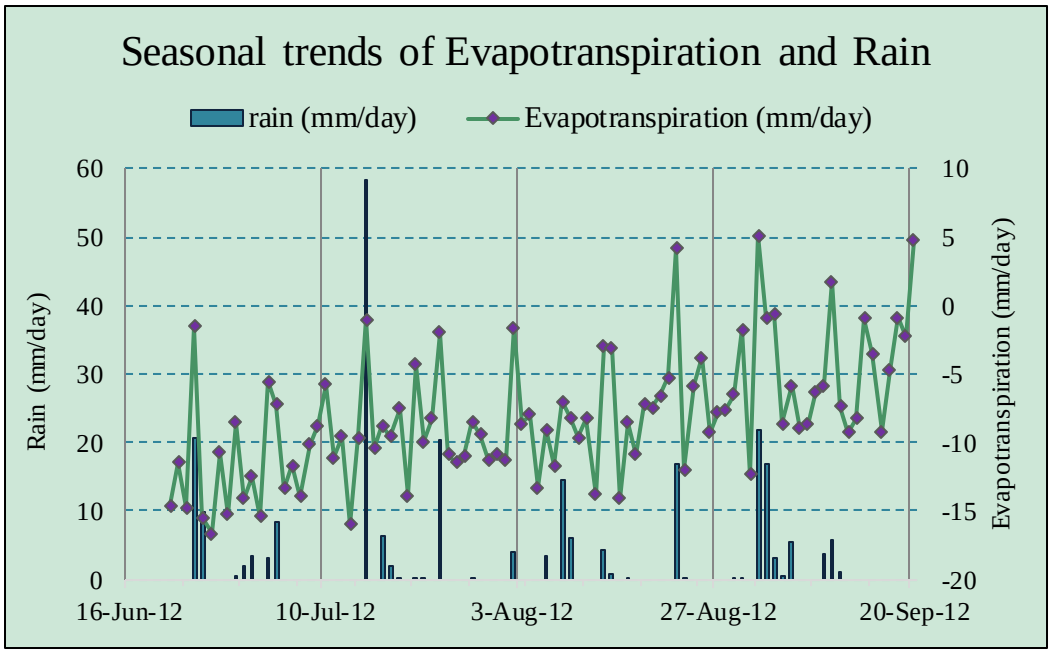


Figure 11. Seasonal trends of Evapotranspiration and Rain in the weather station.

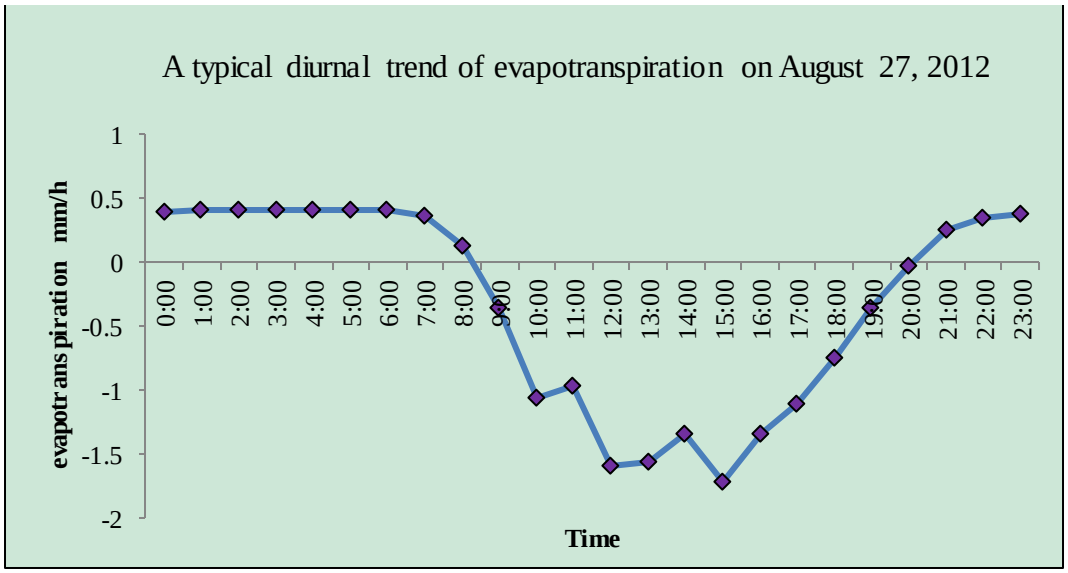


Figure 12. A typical diurnal trend of evapotranspiration in the weather station on August 27, 2012. Negative evapotranspiration indicates water losses to the atmosphere. Positive evapotranspiration indicates water gain for the vegetation due to rain, dews, and fogs.

## Radar image processing

### Preprocessing

Radarsat-2 images were ordered via Acquisition Planning Tool software from MacDonald Dettwiler and Associates (MDA) Geospatial Services Inc. Images of four dates (July 10, August 3, August 27 and September 20) were acquired in the descending orbit at 8 am Mountain Time Zone (14:00 UTC/GMT). These products come in GeoTIFF format and the processing level was SAR Single Look Complex (SLC). The incidence angle is 21.10 degrees. The radiometric error is less than 1 decibel (dB) (MacDonald Dettwiler Associates Ltd 2011). The nominal image coverage (ground range x azimuth) is 25 km x 25 km, as shown in Figure 13. The image covers 56.15 ~ 56.45 °in latitude and -115.03 ~ -115.56 °in longitude. The scene centre is 56 °17'59" N and 115 °18'01" W. Pixel size is ~5 m.

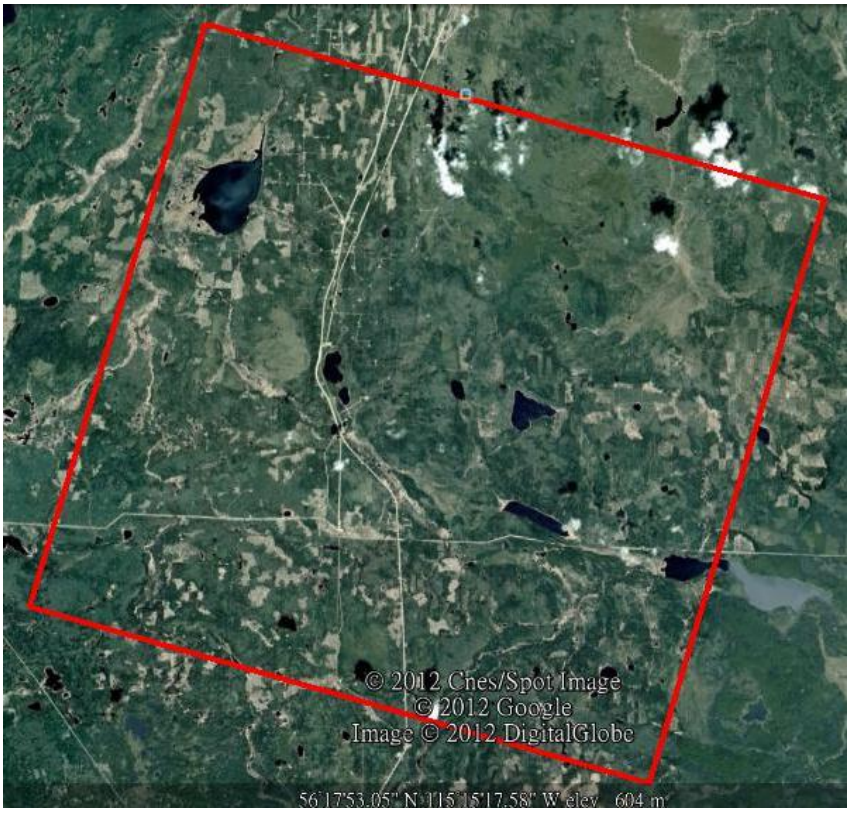


Figure 13. Google image showing the Radarsat-2 acquiring range.

**Image processing**

Non-polarimetric analysis was performed to extract backscattering coefficients from Radarsat-2 images in NEST software (http://nest.array.ca/web/nest, version 5.05 beta) developed by Array Systems Computing Inc. All images went through the same processing steps. First the images were subsetted. Next, multilook was applied for all images with the default setting in NEST. The images were then filtered with Refined Lee filter built in NEST. Later, all images were orthorectified with SRTM 3sec DEM built in NEST. The radiometric correction was also done in this step. Later, all images were further processed with ENVI software developed by Exelis VIS Inc. The images were stacked together according to their polarizations and dates. Finally, the stacked image was further georectified with topographic maps (CanVec) from Natural Resources Canada (NRCan) (Natural Resources Canada 2013). The plot layout was overlaid over the final

stacked image as well as the fire perimeter, as shown in Figure 14. The fire perimeter showed all the 1980s fires in central Alberta. This final resolution (pixel size) was ~12m.

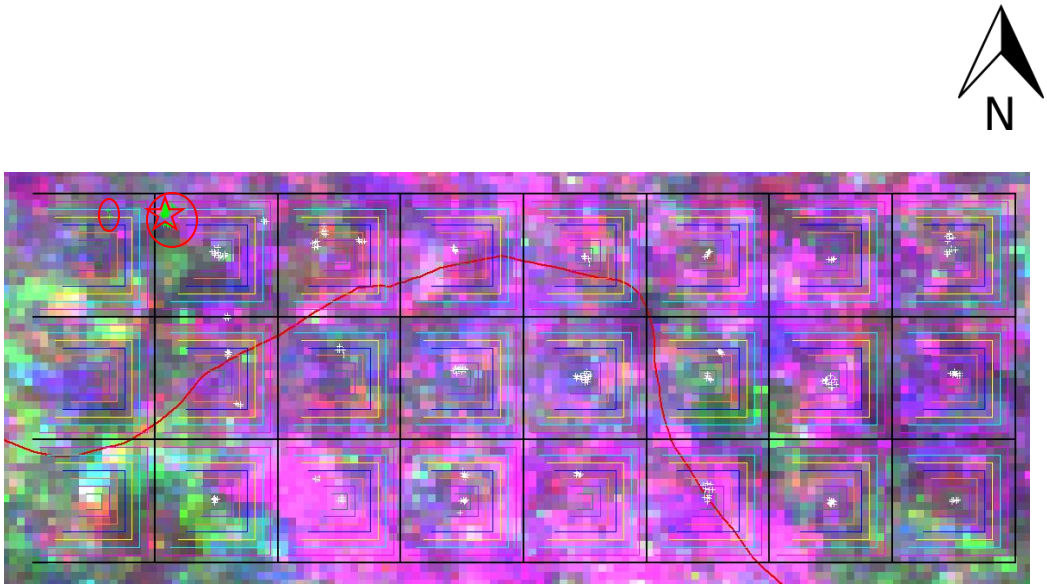


Figure 14. Radarsat-2 polarization color composited image, with HH coded as red, HV as green and VV as blue for August 3, 2012. The red star shows the location of the weather station. The red irregular line is the fire perimeter. The area above the red line was burned in 1980s. The white and green crosses show the field sampling points (peat cores, theta probe and TDR). The green crosses within the red circles show the peat cores, theta probe and TDR samples from Plot 1.

A schematic figure is shown in Figure 15 to demonstrate idealised burned and unburned plots and the plot ID. Figure 16 and Figure 17 are presented to show the in-site view of burned plots while Figure 18 is to show the unburned plots.

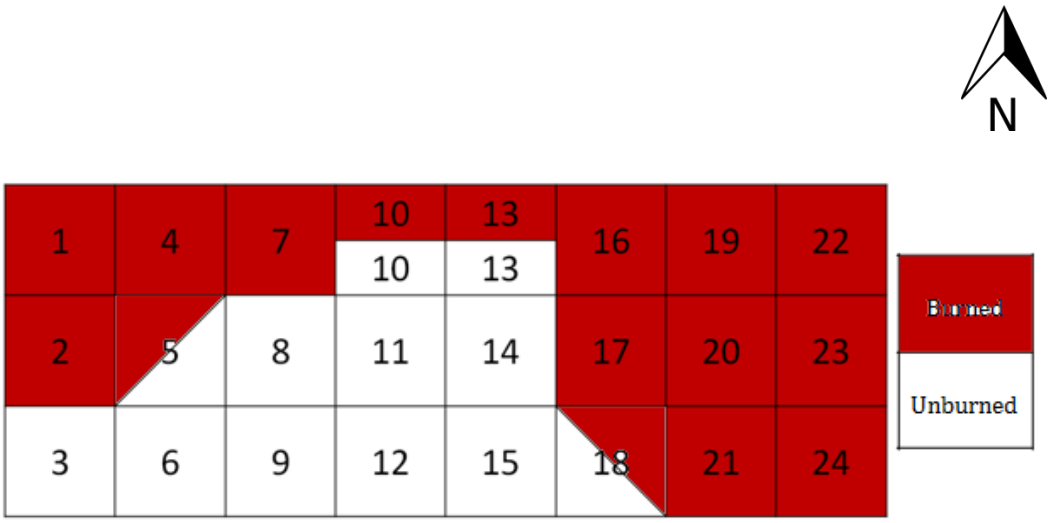


Figure 15. Plot layout. The red plots denote the burned plots.

Figure 16. Plot 20 showing the burned plot and overall landscape of this study area. Photo taken on June 20, 2012.

Figure 17. Plot 24 showing the burned plot. The red flag indicates the center of this plot. Photo taken on June 20, 2012.

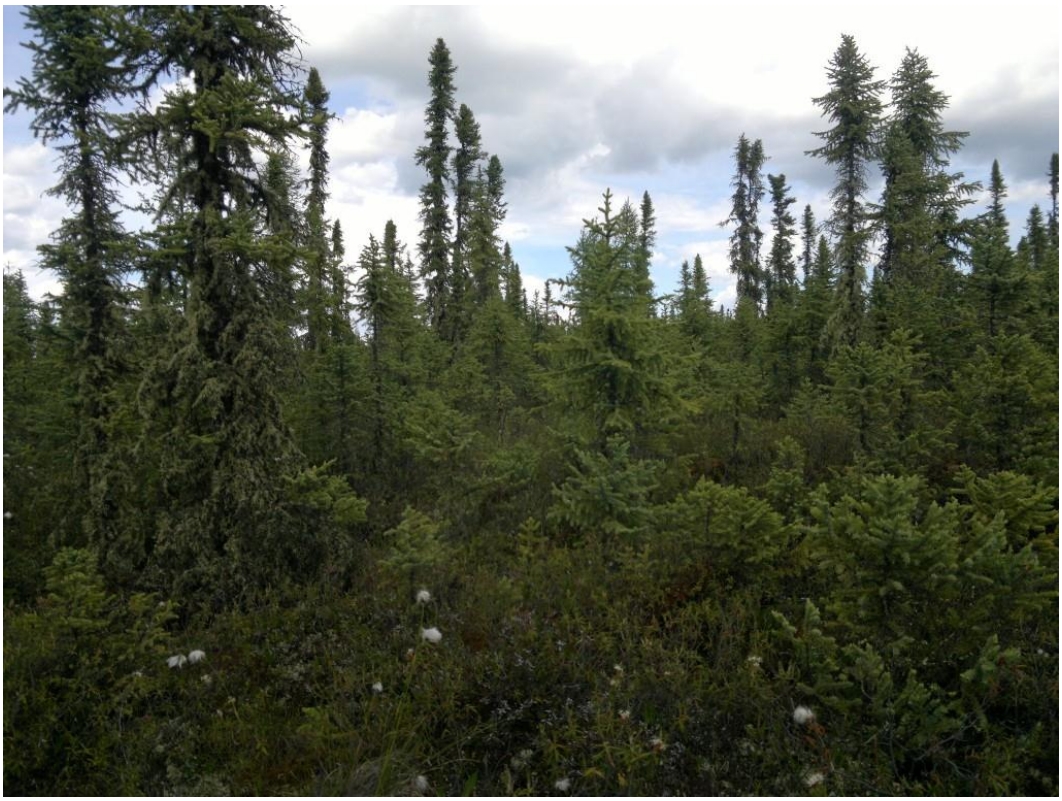

Figure 18. Plot 11 showing the unburned plot. Photo taken on June 20, 2012.

## Ground sampling scheme

Field campaigns took place to coincide with the radar image acquisition. Near the center of each plot, three peat cores and three theta probe readings were taken. In total there were 261 sampling crosses, with 174 for peat cores, 79 for theta probes, as shown in Figure 14. Some sampling crosses are merged together and only represented by one due to the image pixel size.

### Peat cores

Near the center of each plot, three peat cores and three theta probe readings were taken. The exception was on August 27, when the theta probe was unavailable, six peat

cores were taken instead. The coordinates of all peat cores and theta probe readings were recorded with a Garmin[2] GPS (accuracy: within 5 meters).

The peat cores were taken using the cutting-ring method. Each peat core was 5 cm in depth. All peat cores were transferred back to the Fire Ecology Lab in University of Alberta and were oven dried at 65℃ for 48 hours to derive the Gravimetric Moisture Content (GMC). Then together with bulk density, Volumetric Moisture Content (VMC) was calculated with Equation 1.

VMC=GMC* bulk density/pure water density Equation 1.

**Theta probe**

Three theta probe readings were taken besides the peat cores (model type: ML2X, accuracy: 1% VWC). A theta probe is a type of Frequency Domain Reflectometry (FDR) probe: it generates a 100 MHz sinusoidal signal along the array of 4 rods of the probe to the peat. Part of the incident signal is reflected back along this rods array. This reflected signal is a function of the impedance, which almost solely depends on the dielectric constant of the peat at 100 MHz (Delta-T Devices Ltd 1999). Also, as mentioned above, soil moisture is directly in proportion to its dielectric constant, so the reflected signal is closely related to VMC. The reflected signal then interacts with the incident signal, causing a voltage standing wave (Gaskin and Miller 1996). Theta probe measures the output voltage, which is proportional to the difference in amplitude of voltage standing wave (Delta-T Devices Ltd 1999). Therefore, it is possible to convert the microvolts to VMC with a calibration equation described in the theta probe user manual (Delta-T Devices Ltd 1999).

The parameters needed for the calibration came from field dataset of September 20. On that day, the theta probe was inserted into the peat cores, which were later taken back to the lab. This was to obtain the fresh readings. Later, the theta probe was inserted into the oven-dried peat cores to obtain the dry readings. Together with bulk density, the

[2] Mentions of manufacturers or model type are for the convenience of readers only and imply no endorsement on the part of the author. This applies to all brand names appeared in this thesis.

parameters can be determined. With these parameters, VMCs obtained from the theta probe for the other 3 sampling dates were also calculated.

**TDR**

As shown in Figure 14, there are eight Water Content Reflectometers (Model type: Campbell Scientific CS616). The precision of CS616 Water Content Reflectometer is 0.05% VWC, and the resolution is 0.1% VWC (Campbell Scientific Inc. 2002). The CS616 is a type of Time Domain Reflectometry (TDR) probe: it measures the travel time of an electromagnetic pulse (frequency: ~70 MHz in free air, depending on the VMC of the medium) along the rods of the probe through the soil (Campbell Scientific Inc. 2003). Based on the travel time, the velocity can be calculated. Because the velocity is dependent on the dielectric constant of the medium surrounding the rods and VMC is greatly influenced by the dielectric constant (Topp et al. 1980), it is then possible to convert the travel time (microseconds) to VMC with a calibration equation (Hansson and Lundin 2006).

Here are the detailed steps of calibration. First the dielectric constant of water was calibrated as a function of temperature with the polynomial function provided by (Wohlfarth 2005), as shown in Equation 2.

$$\varepsilon_w=249.21-0.79069*T+0.00072997*T^2 \quad \text{. Equation 2.}$$

where T represents temperature in kelvin (K) and $\varepsilon_w$ is the dielectric constant of water.

Next, the apparent dielectric constants were calculated from microseconds following Hansson and Lundin's method (Hansson and Lundin 2006). This method was developed to convert microseconds specifically measured by CS616 into the apparent dielectric constants. Based on the three component mixing model from Kellner and Lundin (Kellner and Lundin 2001), VMC was then calculated from the apparent dielectric constants. This method was developed specifically on peats to convert the apparent dielectric constants into VMC.

These eight TDRs were inserted diagonally to measure the top 5 cm peat moisture. Among these TDRs, TDR 1,2,3,4 were inserted into hummocks and TDR 5,6,7,8 were inserted into hollows. All TDRs were attached to a CR1000 datalogger. Measurements from TDRs were recorded every 60 seconds and were averaged hourly. Only VMCs from

8 am to 3 pm Mountain Time Zone were analysed. This time window was chosen because firstly, Radarsat-2 overpassed the study plots at 8 am and secondly, field sampling usually finished around 3 pm. As an example shown in Figure 19, the field sampling elapse is not a significant source of variation of VMC. Given the reasons mentioned above, it is reasonable to represent the VMC of that field sampling date with the average of this time period.

The connections between some TDRs and the datalogger were lost probably due to bumps during transportation and wild animals' attacks in the field. For example, TDR 1 was only able to record until July 2, 2012; TDR 2 and 4 recorded until August 26, 2012. The seasonal trends of VMC measured by TDR and rainfall are shown in Figure 20. A zoom-in view of VMC measured by TDR on 4 field campaign dates is shown in Figure 21.

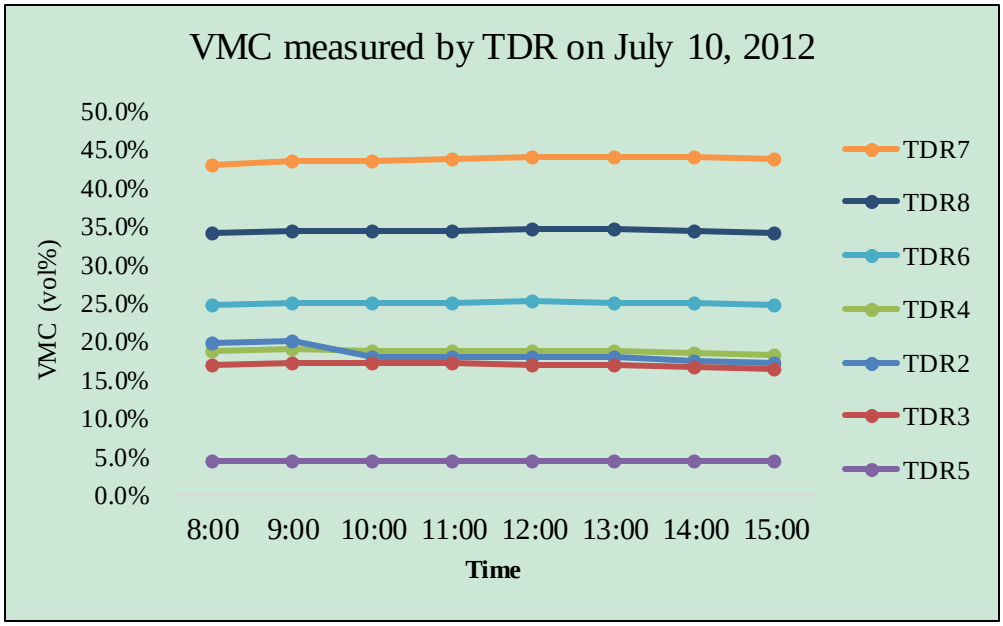


Figure 19. VMC measured by TDR on July 10, 2012. TDR 1,2,3,4 were inserted into hummocks and TDR 5,6,7,8 were inserted into hollows. Figures were not shown for the other 3 field sampling dates due to their similarities.

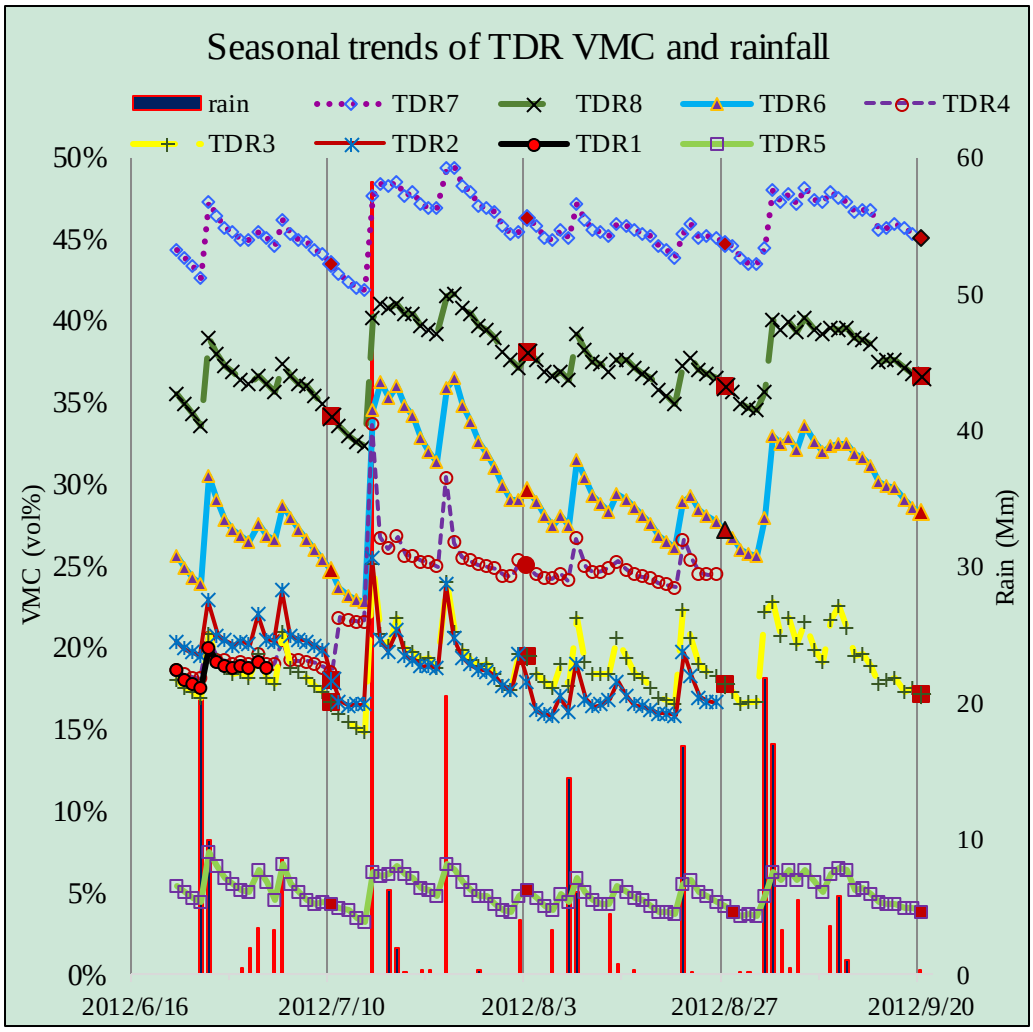


Figure 20. Seasonal trends of VMC measured by TDR and the rainfall. TDR 1,2,3,4 were inserted into hummocks and TDR 5,6,7,8 were inserted into hollows.

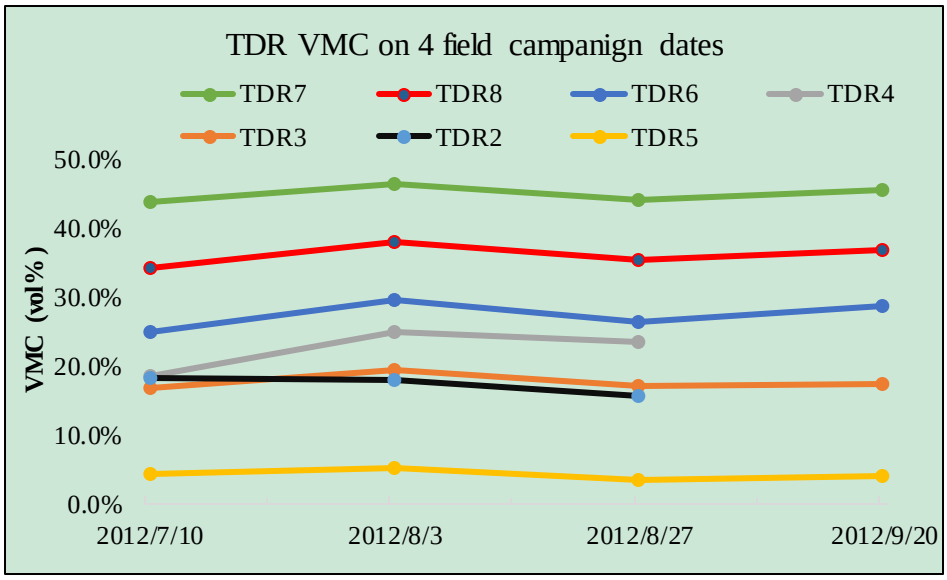


Figure 21. VMC measured by TDR on 4 field campaign dates. TDR 1,2,3,4 were inserted into hummocks and TDR 5,6,7,8 were inserted into hollows.

## VMC retrieval

### Field measured VMC

In order to account for the microtopography (hummocks and hollows) in this bog, VMCs were weighted averaged. To be specific, for a given plot, the VMCs from hummocks were arithmetically averaged as a group and the VMCs from hollows as the other group. The hummock group was given a weight of 0.65 and the hollow group was 0.35. The weight was based on the proportion of hummocks and hollows observed on the site. Then the final VMC for that plot was the sum of the weighted arithmetic mean of the hummock group and the weighted arithmetic mean of the hollow group.

On July 10 and August 3, only peat core samples were taken back to the lab. No field notes were taken about the locations of theta probe readings. Since species can vary greatly even with little topography variation (Vitt and Slack 1975; Rydin 1986), it is not feasible to infer whether those theta probe readings were taken from hummocks or hollows. As a compromise, non-weighted average or arithmetically mean VMCs were used for these 2 sampling dates instead.

On August 27 and September 20, all peat samples (peat cores and theta probes) were taken back to the lab. After species identification, it can be inferred that this peat core was sampled on hummocks or hollows. For example, *Sphagnum fuscum* is almost always found on hummocks in the wild while *Sphagnum angustifolium* and *Sphagnum magellanicum* are found in hollows (Luken 1985; Hogg 1993). In addition, the microtopography (i.e., hummocks or hollows) was recorded for September 20. The species identification results were cross-validated with the field notes. Hence for these two sampling dates, the VMC for any sampled plot was the sum of the weighted arithmetic mean of the hummock group and the hollow group. Usually 0.65 was assigned for the hummock group and 0.35 for the hollow group, unless indicated otherwise by the field notes. For example, it was recorded in the field notes that there was 10% standing water, 60% hummocks and 30% hollows for Plot 21. So the weighted VMC was the sum of 0.6* the arithmetic mean VMC of hummocks and 0.3* the arithmetic mean VMC of hollows and 0.1*100%. 100% is the VMC for standing water.

**Developing the model**

In order to minimise the influence of vegetation, the model was developed based on burned plots. The burned plots were obtained via intersecting the fire perimeter and plots boundaries for 8 scales (25m*25m, 50m*50m, 75m*75m, 100m*100m, 125m*125m, 150m*150m, 175m*175m, and 200m*200m). Half of all the burned plots at 200m scale, together with point samples (peat cores, theta probes and TDRs) from Plot 1, were used to develop the model. VMCs from half of all the burned plots and point samples from Plot 1 were weighed averaged with the method described above. Their corresponded backscattering coefficients were averaged in the same way. The model was built with multiple linear regression in SAS 9.2 (SAS Institute, Cary, NC). The selection criteria were Akaike Information Criterion (AIC) and Root-Mean-Square Error (RMSE).

Here is the general form of the model.

$$VMC=f(p, q) \qquad \text{Equation 3.}$$

where $(p, q) \subseteq (H, V)$, with H, V referred as horizontal and vertical polarization, respectively.

### Retrieving VMC

Based on the developed model, the weighted VMCs of the remaining half of all the burned plots were retrieved. Then also with this model, the weighted VMCs of the unburned plots were also retrieved. Finally, still with this model, the weighted VMCs of all sampled plots were also retrieved. Note, in developing the model and retrieving VMC, half burned plots (Plot 5, 10, 13 and 18) were excluded from both the "burned plots" group and the "unburned plots" group. However, these plots were included in the "all sampled plots" group.

### Validation

Finally, a Pearson's correlation coefficient between the retrieved VMCs and the measured VMCs was calculated with SAS for each sampling day and also for four dates combined. Later, concordance correlation coefficient between the retrieved VMCs and the measured VMCs was calculated with MedCalc 12.5 (MedCalc Software, Ostend, Belgium) for each sampling day and also for four dates combined. The concordance correlation coefficient $\rho$ evaluates the agreement between two variables and examine how close this pair is to the 1:1 line through the origin (Lin 1989). $\rho$ is the product of precision $\rho_r$ and accuracy $a_{cc}$. $\rho_r$ or Pearson correlation coefficient, measures how far each pair deviates from the best-fitted line. $a_{cc}$ measures how far the best-fit line deviates from the 1:1 line through the origin (Lin 1992).

## Results

### Peat cores, theta probes and TDR

VMCs from burned plots for 4 dates combined is shown in Figure 22., with peat cores VMCs as independent variable (x) and theta probe VMCs as dependent variable (y). The peat cores VMCs are the arithmetic mean of the three peat cores taken from a given plot for 4 days combined. A simple linear regression was done with SAS for this dataset and no significant relationship is found at 0.05 level. The medians of the peat cores VMCs and the theta probe VMCs for the burned plots for 4 days combined are 22.2% and 18.9%, respectively.

VMCs from burned plots for 4 dates combined is shown in Figure 23., with the same structure as Figure 22.. No significant relationship is found for this dataset. However, the possibility of failing to reject the null hypothesis is not very high (0.1016), with a RMSE of 0.0521 and $R^2$ of 0.336. The medians of the peat cores VMCs and the theta probe VMCs for the unburned plots for 4 days combined are 23.3% and 14.7%, respectively.

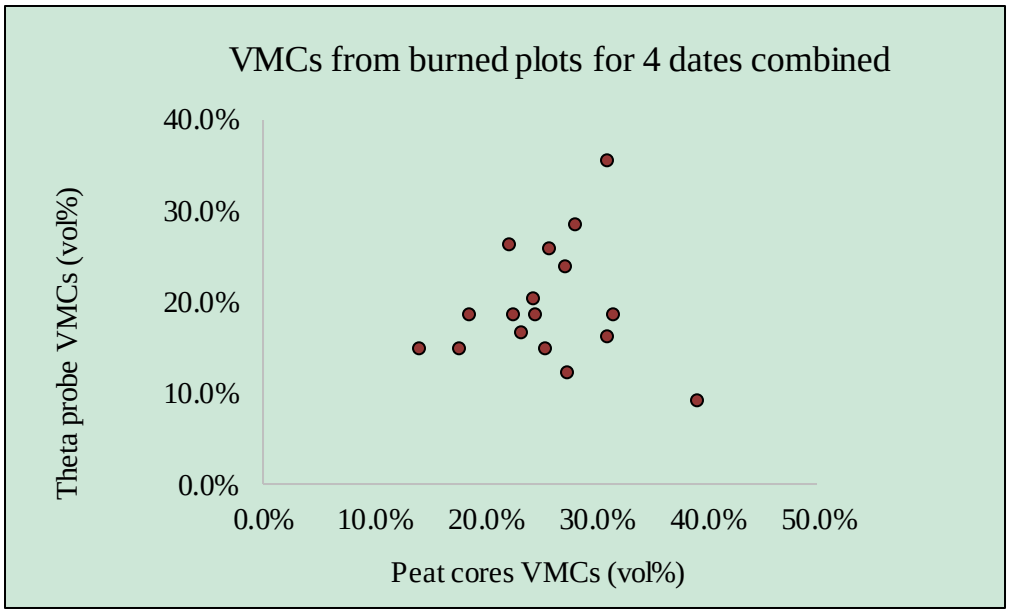


Figure 22. VMCs from burned plots for 4 dates combined.

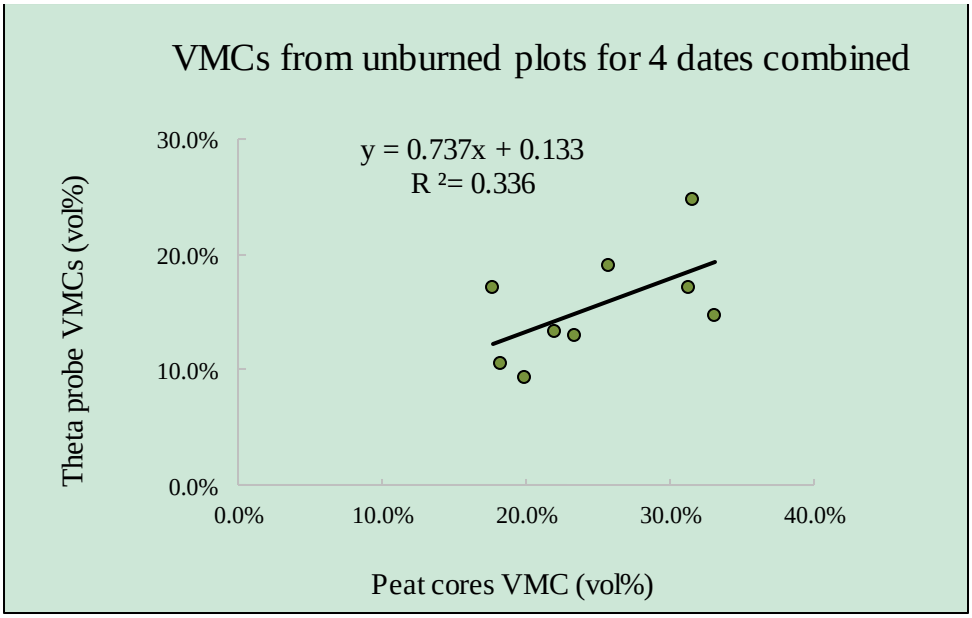


Figure 23. VMCs from unburned plots for 4 dates combined.

Because the theta probe was unavailable on August 27, 2012, the peat cores VMCs from burned and unburned plots are showed in Figure 24. Figure 25 shows the boxplots of VMCs measured by TDR on 4 sampling dates.

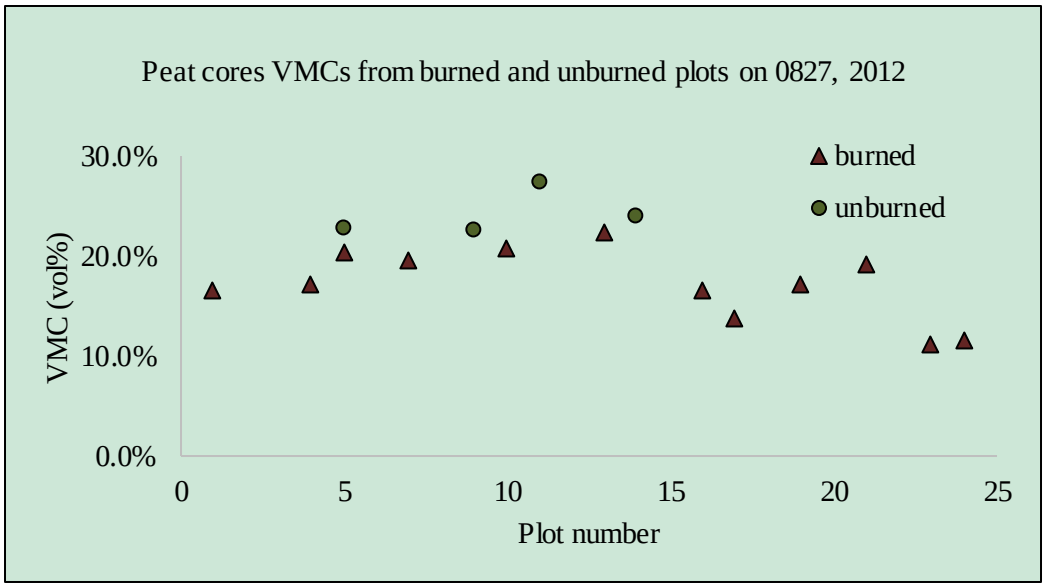


Figure 24. Peat cores VMCs from burned and unburned plots on August 27, 2012

As we can see from Figure 25, on average, VMC is highest on August 3 and lowest on August 27 but the difference among these 4 dates is not large. The majority of VMCs lies in the range of 15% to 35%, same as what peat cores and the theta probe found.

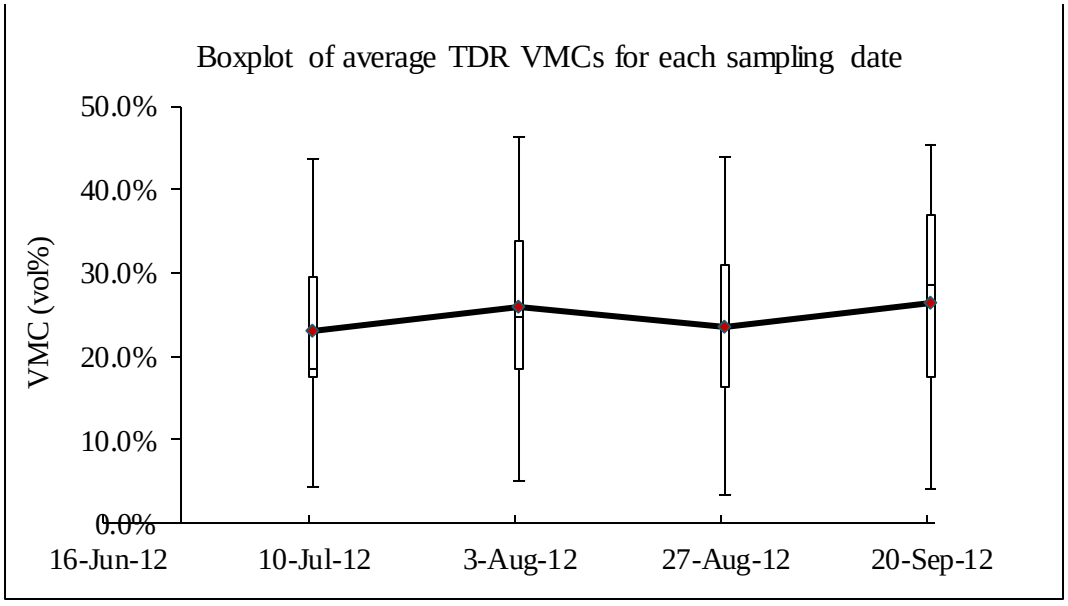

Figure 25.Boxplot of average TDR VMCs for each sampling date. The red rectangular shows the average. The line inside box shows the median. The upper and lower edge of box shows the third quartile (75th percentile) and the first quartile (25th percentile), respectively. The endpoint of the upper and lower whisker shows the maximum and the minimum, respectively.

**Empirical function**

Based on the VMCs of half of all the burned plots at 200m scale, together with point samples from Plot 1 and their corresponded backscattering coefficients, an empirical function was developed with the help of SAS. The function with the smallest AIC and lowest RMSE was selected. Then for the sake of simplicity, the model of 8 variables with an AIC of -112.8148 was selected, instead of the model of 10 variables with a lower AIC of -114.9887.

The final model for the weighted average VMC is as follows:

VMC=-7.59807*HH+5.32491*VV+25.50726*VH-0.75909*HV (dB) +0.78002*VH (dB) +0.18723*VV/VH+0.15379*HH/VH-0.29442*VV/HV Equation 4

Where H, V referred as horizontal and vertical polarization, respectively. Unless followed by dB, all backscattering coefficients in Equation 4 are in the form of intensity. Next, the selected model was tested against the null hypothesis. Since the possibility of failing to reject the null hypothesis is extremely low (<0.0001), this model is used for further VMC retrieval in burned, unburned and all sampled plots combined. Correlation matrices among these polarizations and VMC are shown from Table 1 to 3 to further investigate this model.

Table 1. Correlation matrix for 4 dates combined for burned plots. An asterisk (*) indicates significance at 0.05 level. Same in the following tables.

| | VMC | HH | VV | VH | VH dB | HV | HV dB | $\frac{VV}{VH}$ | $\frac{HH}{VH}$ | $\frac{VV}{HV}$ |
|---|---|---|---|---|---|---|---|---|---|---|
| VMC | 1 | -0.20 | -0.25 | -0.15 | -0.25 | -0.18 | -0.27 | 0.01 | 0.12 | 0.03 |
| HH | -0.20 | 1 | 0.99* | 0.83* | 0.87* | 0.86* | 0.89* | -0.20 | -0.33 | -0.21 |

| | | | | | | | | | | |
|---|---|---|---|---|---|---|---|---|---|---|
| VV | -0.25 | 0.99* | 1 | 0.75* | 0.81* | 0.79* | 0.84* | -0.09 | -0.24 | -0.09 |
| VH | -0.15 | 0.83* | 0.75* | 1 | 0.98* | 0.99* | 0.98* | -0.70* | -0.77* | -0.70* |
| VH dB | -0.25 | 0.87* | 0.81* | 0.98* | 1 | 0.98* | 1.00* | -0.65* | -0.75* | -0.65* |
| HV | -0.18 | 0.86* | 0.79* | 0.99* | 0.98* | 1 | 0.99* | -0.66* | -0.74* | -0.67* |
| HV dB | -0.27 | 0.89* | 0.84* | 0.98* | 1.00* | 0.99* | 1 | -0.60 | -0.71* | -0.61 |
| $\frac{VV}{VH}$ | 0.01 | -0.20 | -0.09 | -0.70* | -0.65* | -0.66* | -0.60 | 1 | 0.98* | 0.99* |
| $\frac{HH}{VH}$ | 0.12 | -0.33 | -0.24 | -0.77* | -0.75* | -0.74* | -0.71* | 0.98* | 1 | 0.97* |
| $\frac{VV}{HV}$ | 0.03 | -0.21 | -0.09 | -0.70* | -0.65* | -0.67* | -0.61 | 0.99* | 0.97* | 1 |

Table 2. Correlation matrix for 4 dates combined for unburned plots.

| | VMC | HH | VV | VH | VH dB | HV | HV dB | $\frac{VV}{VH}$ | $\frac{HH}{VH}$ | $\frac{VV}{HV}$ |
|---|---|---|---|---|---|---|---|---|---|---|
| VMC | 1 | -0.08 | -0.01 | -0.13 | -0.04 | -0.11 | -0.03 | 0.05 | -0.04 | 0.05 |
| HH | -0.08 | 1 | 0.99* | 0.74* | 0.77* | 0.75* | 0.79* | 0.34 | 0.27 | 0.38 |
| VV | -0.01 | 0.99* | 1 | 0.74* | 0.78* | 0.75* | 0.79* | 0.33 | 0.25 | 0.39 |
| VH | -0.13 | 0.74* | 0.74* | 1 | 0.99* | 1.00* | 0.98* | -0.33 | -0.38 | -0.29 |
| VH dB | -0.04 | 0.77* | 0.78* | 0.99* | 1 | 0.98* | 1.00* | -0.29 | -0.36 | -0.25 |
| HV | -0.11 | 0.75* | 0.75* | 1.00 | 0.98* | 1 | 0.99* | -0.30 | -0.36 | -0.27 |
| HV dB | -0.03 | 0.79* | 0.79* | 0.98* | 1.00* | 0.99* | 1 | -0.26 | -0.33 | -0.22 |
| $\frac{VV}{VH}$ | 0.05 | 0.34 | 0.33 | -0.33 | -0.29 | -0.30 | -0.26 | 1 | 0.99* | 0.99* |
| $\frac{HH}{VH}$ | -0.04 | 0.27 | 0.25 | -0.38 | -0.36 | -0.36 | -0.33 | 0.99* | 1 | 0.97* |
| $\frac{VV}{HV}$ | 0.05 | 0.38 | 0.39 | -0.29 | -0.25 | -0.27 | -0.22 | 0.99* | 0.97* | 1 |

Table 3. Correlation matrix for 4 dates combined for all plots combined.

| | VMC | HH | VV | VH | VH dB | HV | HV dB | $\frac{VV}{VH}$ | $\frac{HH}{VH}$ | $\frac{VV}{HV}$ |
|---|---|---|---|---|---|---|---|---|---|---|
| VMC | 1 | -0.18 | -0.18 | -0.16 | -0.23 | -0.16 | -0.23 | 0.11 | 0.13 | 0.11 |
| HH | -0.18 | 1 | 0.98* | 0.75* | 0.79* | 0.76* | 0.80* | -0.05 | -0.07 | -0.04 |
| VV | -0.18 | 0.98* | 1 | 0.72* | 0.76* | 0.73* | 0.77* | 0.02 | -0.03 | 0.02 |
| VH | -0.16 | 0.75* | 0.72* | 1 | 0.98* | 1.00* | 0.98* | -0.64* | -0.66* | -0.64* |
| VH dB | -0.23 | 0.79* | 0.76* | 0.98* | 1 | 0.98* | 1.00* | -0.61* | -0.64* | -0.60* |
| HV | -0.16 | 0.76* | 0.73* | 1.00* | 0.98* | 1 | 0.98* | -0.62* | -0.64* | -0.63* |
| HV dB | -0.23 | 0.80* | 0.77* | 0.98* | 1.00* | 0.98* | 1 | -0.58* | -0.62* | -0.59* |
| $\frac{VV}{VH}$ | 0.11 | -0.05 | 0.02 | -0.64* | -0.61* | -0.62* | -0.58* | 1 | 0.98* | 0.99* |
| $\frac{HH}{VH}$ | 0.13 | -0.07 | -0.03 | -0.66* | -0.64* | -0.64* | -0.62* | 0.98* | 1 | 0.97* |
| $\frac{VV}{HV}$ | 0.11 | -0.04 | 0.02 | -0.64* | -0.60* | -0.63* | -0.59* | 0.99* | 0.97* | 1 |

**Weighted average for the burned plots**

Based on Equation 4, retrieved VMCs were calculated for 4 sampling dates for the other half of all the burned plots at 8 scales. Then Pearson's r was calculated with SAS between the retrieved VMCs and the measured weighted-average VMCs. Due to a small sample size (only 2 plots), Pearson's r is not possible to calculate for 0710, 0803 and 0920. Pearson's r and P value are shown for 0827 in Table 4 and for 4 dates combined in Table 5.

Table 4. Weighted average for the burned plots for 0827.

| Retrieved VMC / Measured VMC | 25m | 50m | 75m | 100m | 125m | 150m | 175m | 200m |
|---|---|---|---|---|---|---|---|---|
| Pearson's r | 0.915 | 0.956* | 0.997* | 0.974* | 0.948 | 0.863 | 0.892 | 0.857 |
| P value | 0.085 | 0.044 | 0.003 | 0.026 | 0.052 | 0.137 | 0.108 | 0.143 |
| Ob# | 4 | 4 | 4 | 4 | 4 | 4 | 4 | 4 |

Table 5. Weighted average for the burned plots for 4 dates combined.

| Retrieved VMC / Measured VMC | 25m | 50m | 75m | 100m | 125m | 150m | 175m | 200m |
|---|---|---|---|---|---|---|---|---|
| Pearson's r | 0.157 | 0.344 | 0.381 | 0.324 | 0.298 | 0.286 | 0.334 | 0.437 |
| P value | 0.664 | 0.330 | 0.278 | 0.361 | 0.403 | 0.423 | 0.346 | 0.207 |
| Ob# | 10 | 10 | 10 | 10 | 10 | 10 | 10 | 10 |

The concordance correlation coefficient ρ was then calculated with MedCalc between the retrieved VMCs and the measured weighted-average VMCs for 4 sampling dates combined and for 8 scales. Based on the total sum of squares of the difference between the retrieved VMCs and the measured weighted-average VMCs, the best result

comes at 200m scale for 4 dates combined, as shown in Figure 26. Here the "best result" referes to the scale that yields the minimum total sum of squares of the difference. The concordance correlation coefficient ρ is 0.435, with an accuracy of 0.997. These numbers indicate a good match between the retrieved and measured VMCs, with data points almost equally and closely distributed above and below the 1:1 line.

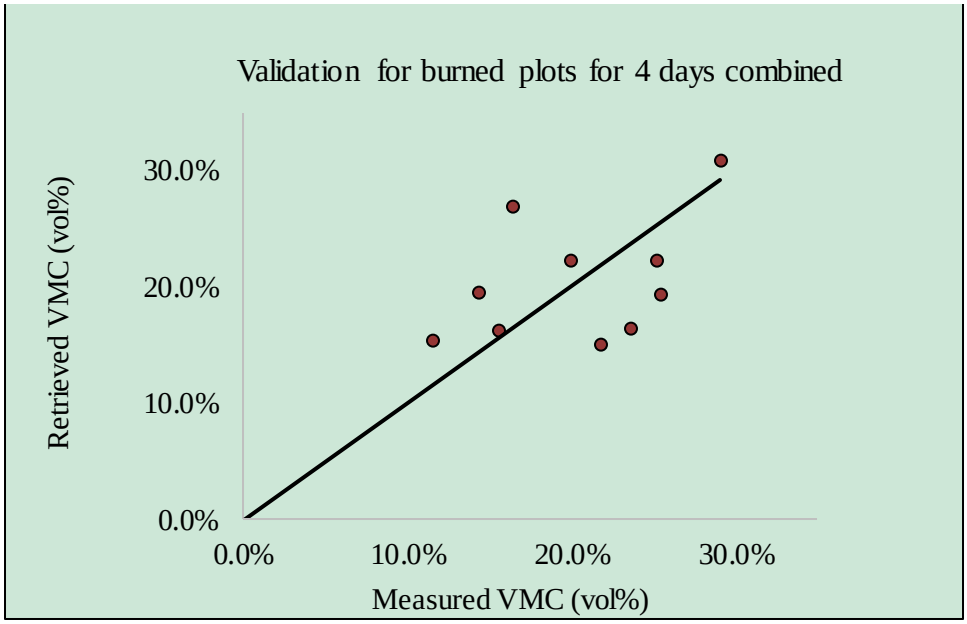


Figure 26. Validation for burned plots for 4 days combined at 200m scale. The solid line shows the 1:1 line through the origin.

**Weighted average for the unburned plots**

Based on Equation 4, retrieved VMCs were calculated for the unburned plots for 4 sampling dates at 8 scales. Then Pearson's r was calculated with SAS between the retrieved VMCs and the measured weighted-average VMCs. Due to a small sample size (only 2 plots), Pearson's r is not possible to calculate for 0710. Pearson's r and P value for the other 3 dates and 4 dates combined are shown from Table 6 to Table 9.

Table 6. Weighted average for the unburned plots for 0803.

| Retrieved VMC / Measured VMC | 25m | 50m | 75m | 100m | 125m | 150m | 175m | 200m |
|---|---|---|---|---|---|---|---|---|
| Pearson's r | 0.108 | -0.049 | -0.281 | -0.423 | -0.397 | -0.373 | -0.308 | -0.277 |
| P value | 0.892 | 0.951 | 0.719 | 0.577 | 0.603 | 0.627 | 0.692 | 0.723 |
| Ob# | 4 | 4 | 4 | 4 | 4 | 4 | 4 | 4 |

Table 7. Weighted average for the unburned plots for 0827.

| Retrieved VMC / Measured VMC | 25m | 50m | 75m | 100m | 125m | 150m | 175m | 200m |
|---|---|---|---|---|---|---|---|---|
| Pearson's r | 0.977 | 0.985 | -0.988 | -0.947 | -0.824 | -0.900 | -0.916 | -0.999* |
| P value | 0.136 | 0.109 | 0.100 | 0.208 | 0.384 | 0.288 | 0.262 | 0.027 |
| Ob# | 3 | 3 | 3 | 3 | 3 | 3 | 3 | 3 |

Table 8. Weighted average for the unburned plots for 0920.

| Retrieved VMC / Measured VMC | 25m | 50m | 75m | 100m | 125m | 150m | 175m | 200m |
|---|---|---|---|---|---|---|---|---|
| Pearson's r | -0.438 | -0.962 | -0.405 | -0.889 | -0.823 | -0.654 | -0.622 | -0.566 |
| P value | 0.712 | 0.176 | 0.735 | 0.303 | 0.385 | 0.547 | 0.573 | 0.617 |
| Ob# | 3 | 3 | 3 | 3 | 3 | 3 | 3 | 3 |

Table 9. Weighted average for the unburned plots for 4 dates combined.

| Retrieved VMC / Measured VMC | 25m | 50m | 75m | 100m | 125m | 150m | 175m | 200m |
|---|---|---|---|---|---|---|---|---|
| Pearson's r | -0.018 | -0.304 | -0.295 | -0.351 | -0.387 | -0.361 | -0.333 | -0.309 |
| P value | 0.956 | 0.337 | 0.351 | 0.264 | 0.214 | 0.249 | 0.291 | 0.329 |
| Ob# | 12 | 12 | 12 | 12 | 12 | 12 | 12 | 12 |

The concordance correlation coefficient was then calculated with MedCalc between the retrieved VMCs and the measured weighted-average VMCs for 4 sampling dates combined and for 8 scales. Based on the total sum of squares of the difference between the retrieved VMCs and the measured weighted-average VMCs, the best result comes at 200m scale for 4 dates combined, as shown in Figure 27. The concordance correlation coefficient $\rho$ is -0.254, with an accuracy of 0.821. These numbers indicate that VMCs are underestimated (more data points are under than above the 1:1 line). This is expected since the model was built based on the burned plots, without much contribution from the vegetation.

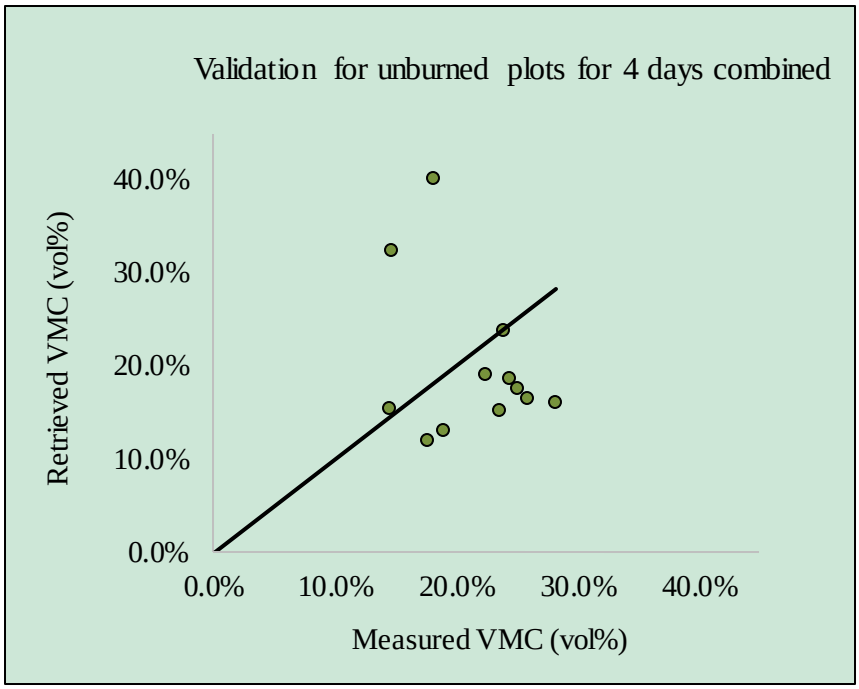


Figure 27. Validation for unburned plots for 4 days combined at 200m scale. The solid line shows the 1:1 line through the origin.

**Weighted average for all plots**

Based on Equation 4, the retrieved VMCs were calculated for all plots for 4 sampling dates. Then Pearson's r was calculated with SAS between the retrieved VMCs and the measured weighted-average VMCs. Pearson's r and P value are shown from Table 10 to Table 14.

Table 10. Weighted average for all sampled plots for 0710.

| Retrieved VMC / Measured VMC | 25m | 50m | 75m | 100m | 125m | 150m | 175m | 200m |
|---|---|---|---|---|---|---|---|---|
| Pearson's r | -0.585 | -0.819* | -0.449 | -0.321 | -0.295 | -0.211 | -0.187 | -0.160 |
| P value | 0.168 | 0.024 | 0.312 | 0.483 | 0.520 | 0.650 | 0.688 | 0.733 |
| Ob# | 7 | 7 | 7 | 7 | 7 | 7 | 7 | 7 |

Table 11. Weighted average for all sampled plots for 0803.

| Retrieved VMC / Measured VMC | 25m | 50m | 75m | 100m | 125m | 150m | 175m | 200m |
|---|---|---|---|---|---|---|---|---|
| Pearson's r | -0.065 | -0.290 | -0.302 | -0.306 | -0.313 | -0.345 | -0.381 | -0.370 |
| P value | 0.879 | 0.486 | 0.467 | 0.462 | 0.450 | 0.403 | 0.352 | 0.368 |
| Ob# | 8 | 8 | 8 | 8 | 8 | 8 | 8 | 8 |

Table 12. Weighted average for all sampled plots for 0827.

| Retrieved VMC / Measured VMC | 25m | 50m | 75m | 100m | 125m | 150m | 175m | 200m |
|---|---|---|---|---|---|---|---|---|
| Pearson's r | 0.543* | 0.504 | 0.335 | 0.113 | 0.057 | 0.125 | 0.402 | 0.483 |
| P value | 0.045 | 0.066 | 0.241 | 0.701 | 0.846 | 0.672 | 0.154 | 0.080 |
| Ob# | 14 | 14 | 14 | 14 | 14 | 14 | 14 | 14 |

Table 13. Weighted average for all sampled plots for 0920.

| Retrieved VMC / Measured VMC | 25m | 50m | 75m | 100m | 125m | 150m | 175m | 200m |
|---|---|---|---|---|---|---|---|---|
| Pearson's r | -0.176 | -0.139 | -0.153 | 0.155 | 0.345 | 0.337 | 0.196 | 0.063 |
| P value | 0.677 | 0.743 | 0.718 | 0.715 | 0.403 | 0.414 | 0.642 | 0.882 |
| Ob# | 8 | 8 | 8 | 8 | 8 | 8 | 8 | 8 |

Table 14. Weighted average for all sampled plots for 4 dates combined.

| Retrieved VMC / Measured VMC | 25m | 50m | 75m | 100m | 125m | 150m | 175m | 200m |
|---|---|---|---|---|---|---|---|---|
| Pearson's r | -0.016 | -0.053 | -0.091 | -0.009 | 0.104 | 0.170 | 0.178 | 0.160 |
| P value | 0.927 | 0.756 | 0.592 | 0.959 | 0.538 | 0.313 | 0.293 | 0.346 |
| Ob# | 37 | 37 | 37 | 37 | 37 | 37 | 37 | 37 |

The concordance correlation coefficient was then calculated with MedCalc between the retrieved VMCs and the measured weighted-average VMCs at 8 scales. Based on the total sum of squares of the difference between the retrieved VMCs and the measured weighted-average VMCs, the best result for 4 dates combined comes at 200m scale for all sampled plots, as shown in Figure 28. The concordance correlation coefficient ρ is 0.153, with an accuracy of 0.962. These numbers indicate that VMCs are underestimated (more data points are under than above the 1:1 line). This is expected since the model was built based on the burned plots, without much contribution from the vegetation.

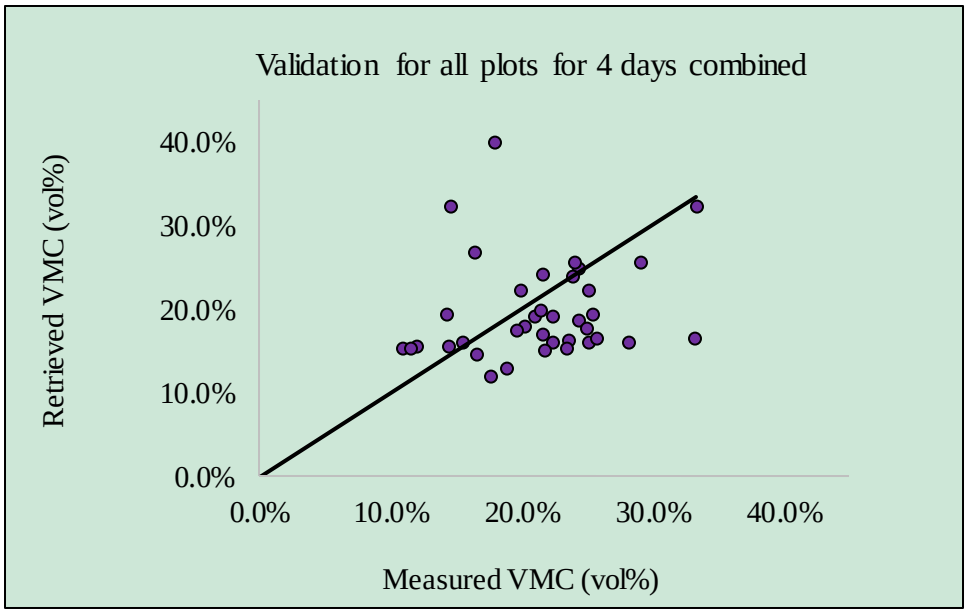


Figure 28. Validation for all plots for 4 days combined at 200m scale. The solid line shows the 1:1 line through the origin.

# DISCUSSION

This research demonstrates that Radarsat-2 is suitable for retrieving VMCs in non-permafrost bogs, especially in burned bogs. Based on Figure 26, Figure 27 and Figure 28, good validation results were achieved for retrieving volumetric moisture contents for the burned plots (accuracy: 0.9967), followed by all sampled plots (accuracy: 0.9618) and unburned plots (accuracy: 0.8208). Some interesting results emerged in this research and are discussed as below. Later, methods of improvement are proposed. Finally the implication for future fire management in peatlands are proposed.

## VMCs measurements

As mentioned in the results, VMCs from the theta probe are lower than that from peat cores. This is in agreement with results found by (Blanc and Dick 2003), who suggested this may be because of soil compression caused by inserting rods of the probe and loose contact between the soil and the rods. However, as also pointed in (Blanc and Dick 2003), depending on the soil structure, soil compression may lead to an overestimation of VMCs (Robinson et al. 1999). It is suggested that the overestimated VMCs measured by the theta probe are probably due to soil compaction near the electrodes and the strong bias in the sensitivity of the regions near the central electrode (Robinson et al. 1999). Another possible reason for this contradictory result may be due to the difference in model type. Though in all three cases, the device was produced by the same company (Delta-T devices, Burwell, Cambridge), Robinson et al. used Model ML-01 while here ML2X is used. No model type was mentioned in (Blanc and Dick 2003), though. ML2X is an advanced version of ML-01 and would give slightly higher or equal outputs, everything else being equal (Delta-T Devices Ltd 1999).

Apart from the influence of soil compaction, loose contact, sensitivity biases of the rods and the device model itself, other factors such as spatial variation and temperature, may also attribute to the differences between VMCs obtained via the theta probe and peat cores.

### Spatial variation

The inherent nature of this spatial variation seems likely to be another factor (Kaleita et al. 2005; Melloh et al. 2006). In this research, theta probe readings were not taken at

exactly same place where peat cores were taken except for part of the September 20 dataset. For September 20, for calibrating the theta probe, half of the peat cores were taken where the theta probe readings were recorded. Hence it is likely that the theta probe did not even measure VMCs from same moss species as that from peat cores, since species can vary greatly even with little topography variation (Vitt and Slack 1975; Rydin 1986). In addition to the species variation, the spatial variation can also mean the differences in the moisture content of *Sphagnum* mosses since moisture can fluctuate a lot within the live and dead layers of *Sphagnum* mosses (Yoshikawa et al. 2004). Furthermore, this spatial variation could also indicate the differences in moss porosity, moss stem and leaf and moss salinity (Yoshikawa et al. 2004). Future work is required to quantify the impact of this spatial variation.

**Temperature**

As show in Figure 10, the temperature during the sampling season ranges roughly from 5 to 25℃ (278.15 to 298.15 K). In this range, according to Equation 2 in (Wohlfarth 2005), as temperature increases, the dielectric constant of water decreases. Since the dielectric constant of water is way more important than that of soil and air (~80 for water, ~5 for dry soil and ~1 for air), any changes in the dielectric constant of water will make a huge impact on the overall dielectric constant of peats. Though due to the binding force in the peat matrix, the dielectric behavior of pure water is not identical to that out of the peat (Escorihuela et al. 2007), it can still be inferred that the temperature impact on the overall dielectric constant of peats shall not be overlooked. Especially in this research, the theta probe was calibrated with the September 20 dataset, when the temperature is lowest during the field season and hence the dielectric constant of water is the highest. Given that the dielectric constant is directly in proportion to VMC (see Figure 3), this temperature effect on the dielectric constant of water would like be an important cause of the lower VMCs obtained via the theta probe than that via peat cores, especially for July 10 and August 3 datasets. This temperature effect was taken account during the TDR calibration process.

Another possible effect of temperature is its influence on the bound vs. free water. The liquid water in the peat matrix can be divided into free and bound water. Bound water has a much lower dielectric constant compared with that of free water (~3 for bound water and ~80 for free water) (Dobson et al. 1985; Nagare et al. 2011). For the

theta probe, it can hardly measure that bound water's contribution. By contrast, for VMCs obtained via oven dried (65℃) peat cores, it is very likely that the bound water proportion such as intra-cellular solution is also included (Overduin et al. 2005). The influence of bound water alone, however, is believed to be minimal on calibrating VMCs due to its negligible volumetric proportion in low bulk density peats (Nagare et al. 2011). But when compared with VMCs obtained via peat cores, this influence is likely to cause a lower VMC measured by the theta probe.

Apart from the differences of VMCs measured between the theta probe and peat cores, other researchers found that the theta probe alone actually can accurately measure VMCs in custom-made substrates (a mixture of peat, bark, perlite, and vermiculite) (Nemali et al. 2007), and *Sphagnum spp.* mosses (Yoshikawa et al. 2004), under various electrical conductivity and temperature conditions. It is even indicated that the theta probe may be superior to the oven-dried method in terms of accuracy and efficiency (Bosch et al. 2006).

The principle of how theta probe, TDR, and Radarsat-2 measure VMC is all largely based on the large contrast in dielectric constant between free water and soil and they only take the free water into account. Also, these three methods all work under ambient temperature (~15℃). By contrast, the oven dried peat cores takes both the free and bound water into account and works at 65℃. Though oven dried method has long been considered as the "standard" method in measuring VMC in soil science, in this research, it seems that probably TDR and theta probe would be a better choice for the ground measured VMCs and for later comparison with Radarsat-2. Future work is required for further investigation, as discussed in the "Field sampling" under the "Methods of improvement" section.

### Correlation and scales

As seen from the above tables (Table 6--11, 13 and 14), there are negative correlations between the retrieved VMCs and the measured VMCs. This negative correlation is likely caused by the influence of vegetation. The function was developed based on VMCs of half of all the burned plots at 200m scale, together with point samples from Plot 1, which is burned as well. So the influence of vegetation is not very well

represented in the model. This model is suitable for later retrieval VMC for the remaining half of all the burned plots (see Figure 26). However, when it comes to the unburned plots or all sampled plots, this model may not be that accurate since the influence of vegetation is underestimated. This can be further proved from the difference among burned, unburned and all plots and also from the seasonal and scaling difference.

For burned plots, the influence of vegetation is minimized, so no negative correlation is found at any scale on any sampling date (see Table 4 and Table 5). Since the model was developed at 200m scale, in general, the correlation results are best at 200m scale (see Table 5). Nevertheless, since all these correlations are weak and not significant, caution shall be exercised in interpreting these results. Besides, due to a small sample size, no solid conclusion can be drawn from Table 4.

For unburned plots, the influence of vegetation is greatest among these three groups (burned, unburned and all plots combined), so negative correlation is found on all sampling dates at most scales, especially the large scales (100m to 200m) (see from Table 6 to Table 9). At larger scales, the influence of vegetation is stronger than at smaller scales for unburned plots since backscattering coefficients generally increase as the scales increase (data not shown). The contribution from vegetation partly compensates for the weaker backscattering coefficients averaged over a smaller scale. So now instead of 200 m scale, it is at 125m that the best correlation result was achieved (see Table 9). But due to a lack of vegetation sampling, the exact influence of vegetation cannot be quantified. Thus far, no certain answer can be given on what scale works the best for unburned plots. In addition, due to a small sample size, no solid conclusion can be drawn from Table 6 to Table 8. Since all these correlations are weak and not significant, caution shall be exercised in interpreting these results.

For all sampled plots, the result is mixed: on July 10 and August 3, negative correlation is found for all scales (see Table 10 and Table 11); on August 27, no negative correlation is found for all scales (see Table 12); on September 20, negative correlation is found for small scales (25m to 75m) while positive correlation is found for large scales (100m to 200m) (see Table 13). The negative or positive correlation may be a result of the way the model was developed and seasonal dynamics of vegetation.

This model was developed based on VMCs of 4 sampling dates, with each date's contribution equal. For the first two sampling dates, vegetation was lush and verdant in

this mid-summer. However, by the time of sampling in September, vegetation was withered and flaccid in this autumn. This seasonal change of vegetation affects the backscattering coefficients in two ways: one in the scattering mechanisms and the other in the dielectric constant. As the shrubs wilted, the surface scattering, double scattering, and multiple scattering all decreased. In addition, as the shrubs lost water, dielectric constant also decreased, resulting in a decline of backscattering coefficients.

Hence, it can be concluded that the influence of vegetation was greatest on July 10 and August 3 and weakest on September 20. The strong contribution from vegetation in the mid-summer, which probably is heavily underestimated in the model, results in the negative correlation found on July 10 and August 3 at all scales for all sampled plots. By contrast, the small contribution from vegetation in the autumn, which is slightly underestimated in the model, results in the mixed result found on September 20 at 8 scales for all sampled plots. The positive correlation found at larger scales on September 20 for all sampled plots is likely due to the fact that the model was developed at 200m—the largest scale of all the 8 scales. Consequently, the model may better capture the dynamics at larger scales. However, since all these correlations are weak and not significant, caution shall be exercised in interpreting these results.

As for August 27, it is a bit more complex due to its sampling plots and sampling date. On one hand, almost twice the number of plots was sampled compared with the other 3 sampling dates. Hence, twice the number of plots (4 compared 2 plots for any other 3 dates) was entered to develop the model. With a larger contribution to the model, later the dynamics of VMCs for this date (0827) may be better presented in the model. On the other hand, August 27 was in the transition period from mid-summer to autumn. The influence of vegetation was neither too strong, like July 10 and August 3, nor too weak, like September 20. Consequently, given the two reasons mentioned above, we see some negative correlations appeared for the unburned plots but positive for all sampled plots on August 27.

Finally, for all sampled plots for 4 dates combined, a transition from negative correlation to positive is observed (see Table 14). It can be inferred that, based on the reasons mentioned above, at small scales (25m to 100m), the influence of vegetation dominates. Hence, the correlation is negative. As the scale increases, the impact of vegetation becomes "diluted" for burned and unburned plots combined since the burned

plots are quite open, *c.f.* Figure 16. Then the scale effect becomes dominative. Therefore, the correlation is positive. Nevertheless, since all these correlations are very weak and not significant, caution shall be exercised in interpreting these results.

### Empirical model

This research shows that Radarsat-2 can be used to retrieve VMCs in non-permafrost bogs. It works best for the burned plots while slightly underestimates VMCs for the unburned and all plots combined. In addition to the reasons given above, this underestimation is also partly the result of the empirical nature of this method. A thorough analysis of the components (co-and cross polarizations and their combinations) of this model is given below.

As seen from Table 1 to Table 3, different single polarizations (HH, HV, VH, VV in intensity, VH, HV in dB) are strongly and positively correlated with the others for burned, unburned and all plots combined. Polarization combinations correlates strongly and positively within other members for burned, unburned and all plots combined. No single polarizations nor single polarization combinations correlate VMC significantly. This indicates that a single polarization or a single polarization combination is not enough to accurately retrieve surface moisture.

As shown in Table 1, for burned plots, polarization combinations (VV/VH, HH/VH and VV/HV) are not significantly correlated with co-polarizations (HH, VV) but do strongly and negatively with cross-polarizations (VH, HV and their dB forms). As shown in Table 2, for unburned plots, polarization combinations are not significantly correlated with co-polarizations nor cross-polarizations. As shown in Table 3, for all plots combined, polarization combinations are not significantly correlated with co-polarizations but do strongly and negatively with cross-polarizations.

In this model, cross-polarizations seem to be important components, especially VH since the model contains both its intensity and dB forms. This is in agreement with (Bourgeau-Chavez et al. 2013b), where they also find that VH is the dominative polarization in the moisture prediction models for unburned plots and all plots combined. Besides, VH is also sensitive to surface roughness, as shown in Figure 3 (a) in (Oh 2004). Also shown in (Oh 2004),VV/VH is insensitive to soil moisture but very sensitive to

surface roughness. HH and VV are also found to be sensitive to soil moisture and surface roughness and also vegetation (Wang et al. 2000). So the possible explanation for this empirical function is that some polarizations and/or their combinations account for the influence of soil moisture, some for surface roughness and others for vegetation. Since the influence of moisture, surface roughness and vegetation are intertwined, their corresponded polarizations are also highly correlated, as analysed above. By combining different polarizations together, this empirical function can successfully retrieve surface moisture. However, due to its empirical nature and no target decomposition, caution shall be exercised in interpreting these results.

This research retrieved surface peat moisture empirically to bypass the difficulties encountered in theoretical models (Dubois et al. 1995). This empirical approach is suitable for complex natural ecosystems such as boreal peatlands which have multiple scattering mechanisms (Bourgeau-Chavez et al. 2013a). Nevertheless, this method does not come without limitations. Due to its empirical nature, this function is limited to this study area or other similar landscapes. If other researchers would like to apply this method in different ecozones or during a different time period, they need first to train the model with a relatively large dataset in order to represent the local spatial and temporal variabilities. The need to fitting eight variables (or potentially even more) every time can be an impediment for a fast application in fire hazard monitoring. Thankfully, with the advance in Information Technology, the computing power is increasing dramatically. It is expected in the near future, even with a basic laptop, such modeling task can be performed quickly.

## Methods of improvement

Under ideal circumstances, this experiment result can be potentially improved by more field sampling and image fusion.

### Field sampling

If more field assistants were available, more peat cores and plots could be sampled. Given more experience and resources, it is possible to extend the field season by both starting earlier like May and ending later like October. If resources allowed, a long term experiment could be set up to investigate the yearly fluctuation of surface peat moisture via SAR after wildfire, as shown in (Kasischke et al. 2007). With more data available, a

larger dataset would be allocated to develop the equations instead of only half of all the burned plots. With a larger dataset over a longer period of time, the equations developed may better capture the peat moisture dynamics. Later in the retrieval and correlation sections, the results may be improved.

With more plots sampled, a larger dataset would be allocated for better calibrating the theta probe. Compared with TDR, the theta probe has a relatively short history of research. For example, the prototype of TDR was first developed in 1980s (Topp et al. 1980) while the first prototype of theta probe was proposed almost two decades later (Gaskin and Miller 1996). While TDR has well thought-out calibration models such as the three component mixing model (Kellner and Lundin 2001), the theta probe is still relative new and under development. In addition, most researchers focus on the mineral soils and only a few on the peats (Nagare et al. 2011). The good news is that as the technology advances, the theta probe is improving. The newly introduced model type ML3 comes as a replacement of ML2X, enabling simultaneous recording of soil temperature with soil moisture (Delta-T Devices Ltd 2013). It can be expected that in the near future, better calibration model will be developed to incorporate the temperature influence and hence more accurate measurements can be achieved by the theta probe.

With more samples available, another method—change detection, can be applied to estimate peat moisture content. Change detection is to quantify the temporal changes of an object (surface peat moisture in this research) with the application of multi-temporal datasets (Lu et al. 2004). In surface moisture retrieval, it is assumed that, ideally, the changes of surface roughness and vegetation are minimal throughout the experiment period (Wickel et al. 2001) and the only factor that would change is the surface moisture content. In reality, the surface roughness can be constant, providing no wildfires take place. However, given the 24-day revisit time of FQ3 beam mode adopted in this research, boreal vegetation will almost inevitably change in reflectance due to species phenology, foliar and other seasonal influences (Miller et al. 1997). As mentioned before, field sampling and models such as WCM and IEM are required to implement change detection. However, such approach is not feasible thus far.

**Image fusion**

Another possible way to even further improve the result is image fusion, i.e., combining SAR data from different bands with optical/infrared images. This could

potentially solve the conflict between spatial and temporal resolution. Here, the conflict refers to the fact that images with a short revisit time often comes at a coarse spatial resolution. With a single remote sensing image source, resources managers have to carefully balance the need for timely update and the need for high spatial resolution and find the balance point inbetween.

However, provided with more remote sensing image sources, this conflict can be solved and can even result in improved accuracy of surface moisture retrieval. Some examples are (Wang and Qi 2000; Wang et al. 2004), where C band and optical images are synergized. A schematic flowchart (Figure 29) is to show the outline of radar and optical image fusion at decision level. For more details about the concepts, methods and applications of image fusion, readers are advised to refer (Pohl and Van Genderen 1998).

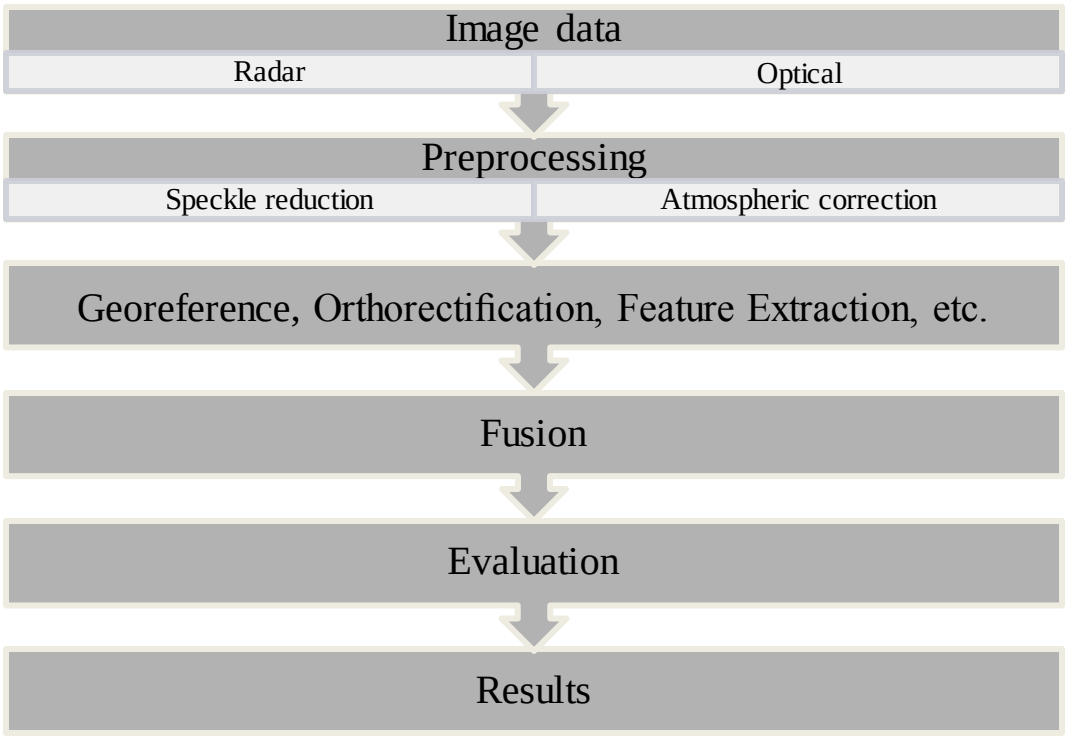


Figure 29. Outline of radar and optical image fusion at decision level, adapted from (Pohl and Van Genderen 1998).

While image fusion may yield better results, image availability still remains one of the major constraints for executing such project (Warner 2010). With more remote sensing images at hand, researchers are required to be even more knowledgeable. This

may set barriers especially for the beginning researchers. In addition, usually it is not economically-feasible to acquire various sources of images. As put in (Bryant et al. 2003), optical images such as Landsat archive images are free but are subjected to poor weather conditions and day time acquisition only; Thermal infrared images from MODIS Thermal Infrared (TIR) bands are inexpensive but often come at coarse spatial resolution; SAR images from Radasat-2 come at high spatial resolution and usually not impacted by weather but usually way more expensive than the other two. The good news is that with the Science and Operational Applications Research (SOAR) program from CSA and MDA, Radarsat-2 images are offered free of charge for selected researchers (Soria-Ruiz et al. 2007). This will help explore Radarsat-2's new contributions to various Earth observations including surface moisture retrieval. Another good news is that as ALOS-2 PALSAR (L-band) and Sentinel-1 SAR (C-band) will launch in the coming few years, the research community will then have more opportunities to further explore the advantages of SAR in retrieving surface peat moisture.

### Implications for future fire management

Given the importance of peat fires and no moisture code specifically for the peatlands (Waddington et al. 2012), Peat Moisture Surface Code (PMSC) and Peat Moisture Ground Code (PMGC) are now conceptually proposed to better represent the moisture dynamics for remote sensing in non-permafrost continental peatlands. PMSC can correspond roughly to a combination of FFMC and DMC, referring the moisture of the top ~5cm layer of peat mosses, lichens, stunted shrubs, etc. This layer usually is porous, loosely compactly, alive or decomposing and corresponds to the depth that Radasat-2 and other C-band space-borne SARs can penetrate and measure. Also this layer is critical in initializing the surface fire. PMGC can correspond roughly to DC, referring the moisture of the 10~20cm layer of the peat, plant residuals, etc. This layer usually is compact, decomposing and humified and corresponds to the depth that ALOS-2 (under construction) and other L-band space-borne SARs can penetrate and measure. Also this layer is critical in sustaining smouldering combustion.

The way to calculate surface peat moisture and ground peat moisture is the same as how VMCs were obtained via Radarsat-2 in this research. Then these VMCs will be scaled empirically into 5 classes of fire danger—extremely low, low, medium, high, and

extremely high. Larger VMCs correspond to a lower class, indicating a lower risk of fire danger and vice versa. Also a threshold will be helpful in real life fire management. Later, a software can be programmed so that PMSC and PMGC will be displayed automatically, along with a figure showing the areas of high fire danger risk. Researchers only need to upload the SAR images of a targeted peatland and other required background information. Then, resources and manpower can be better allocated for fire management in peatlands. This vision will require a cooperation of environmental scientists, ecologists, fire scientists and mangers, government officers, computer scientists, and Geographic Information System (GIS) technicians.

As demonstrated in (Bourgeau-Chavez et al. 1999; Abbott et al. 2007), C band SAR signals correlate significantly with the existed 3 fuel moisture codes in boreal forests, especially with DMC and DC. Also, as demonstrated in (Waddington et al. 2012), it is suitable, though not without limitations, to use the existed 3 fuel moisture codes for predicting fire danger in boreal peatlands. Hence, it is feasible to design PMSC and PMGC in such manner that they can be further integrated into the CFFDRS to predict fire danger in boreal peatlands. In addition, since these two codes are computed directly from space-borne SAR images, they can be updated on a frequent and regular basis for better fire hazard monitoring in peatlands. This is especially vital because the majority peatlands in Canada is located in remote and uninhabited areas. Moreover, it is then feasible to achieve a large spatial coverage with a high spatial resolution and a low cost per square meter. Besides, such data are convenient to scale up or down and accessible to be incorporated into other environmental/ecological models such as carbon budget modeling.

# CONCLUSIONS

In this research, retrieving VMCs with Radarsat-2 in peatlands shows promise for the burned plots (concordance correlation coefficient $\rho$: 0.435; accuracy: 0.997), followed by all sampled plots ($\rho$: -0.254; accuracy: 0.962) and unburned plots ($\rho$: 0.153; accuracy: 0.821). The negative correlation is likely due to the influence of vegetation. Methods of improvement such as field sampling and image fusion are proposed.

Finally two peat moisture codes (PMSC and PMGC) are proposed for future fire management in peatlands. PMSC, which is critical in initialing the surface fire, can be

obtained via C band. PMGC, which is critical in sustaining smouldering combustion, can be obtained via L band. Future work and interdisciplinary collaboration are required to further elaborate and fulfill this proposal.

# BIBLIOGRAPHY


Abbott, K.N., Leblon, B., Staples, G.C., Maclean, D.A., & Alexander, M.E. (2007). Fire danger monitoring using RADARSAT - 1 over northern boreal forests. *International Journal of Remote Sensing, 28*, 1317-1338

Alberta Energy and Utilities Board, & Alberta Geological Survey (1967). Organic soils tour Alberta soil survey. In (pp. 1-39)

Andrejko, M.J., F., L., , & Cohen, A.D. (1983.). Comparison of ashing techniques for determination of the inorganic content of peats. In P.M. Jarrett (Ed.), *Testing of peats and organic soils American Society for Testing and Materials* (pp. 5-20). Philadelphia: ASTM Special Publication

Andrus, R.E., Wagner, D.J., & Titus, J.E. (1983). Vertical zonation of Sphagnum mosses along hummock-hollow gradients. *Canadian Journal of Botany, 61*, 3128-3139

Attema, E.P.W., & Ulaby, F.T. (1978). Vegetation modeled as a water cloud. *Radio Science, 13*, 357-364

Baghdadi, N., Gaultier, S., & King, C. (2002a). Retrieving surface roughness and soil moisture from synthetic aperture radar (SAR) data using neural networks. *Canadian Journal of Remote Sensing, 28*, 701-711

Baghdadi, N., Gherboudj, I., Zribi, M., Sahebi, M., King, C., & Bonn, F. (2004). Semi-empirical calibration of the IEM backscattering model using radar images and moisture and roughness field measurements. *International Journal of Remote Sensing, 23*, 3593–3623,

Baghdadi, N., King, C., Chanzy, A., & Wigneron, J.P. (2002b). An empirical calibration of the integral equation model based on SAR data, soil moisture and surface roughness measurement over bare soils. *International Journal of Remote Sensing, 23*, 4325-4340

Barrett, B.W., Dwyer, E., & Whelan, P. (2009). Soil Moisture Retrieval from Active Spaceborne Microwave Observations: An Evaluation of Current Techniques. *Remote Sensing, 1,* 210-242

Belyea, L.R., & Malmer, N. (2004). Carbon sequestration in peatland: patterns and mechanisms of response to climate change. *Global Change Biology, 10,* 1043-1052

Benscoter, B.W., Thompson, D.K., Waddington, J.M., Flannigan, M.D., Wotton, B.M., de Groot, W.J., & Turetsky, M.R. (2011). Interactive effects of vegetation, soil moisture and bulk density on depth of burning of thick organic soils. *International Journal of Wildland Fire, 20,* 418-429

Benscoter, B.W., & Vitt, D.H. (2008). Spatial Patterns and Temporal Trajectories of the Bog Ground Layer Along a Post-Fire Chronosequence. *Ecosystems, 11,* 1054-1064

Benscoter, B.W., & Wieder, R.K. (2003). Variability in organic matter lost by combustion in a boreal bog during the 2001 Chisholm fire. *Canadian Journal of Forest Research-Revue Canadienne De Recherche Forestiere, 33,* 2509-2513

Benscoter, B.W., Wieder, R.K., & Vitt, D.H. (2005). Linking Microtopography with Post-Fire Succession in Bogs. *Journal of Vegetation Science, 16,* 453-460

Biftu, G.F., & Gan, T.Y. (1999). Retrieving near-surface soil moisture from Radarsat SAR data. *Water Resources Research, 35,* 1569-1579

Bindlish, R., & Barros, A.P. (2001). Parameterization of vegetation backscatter in radar-based, soil moisture estimation. *Remote Sensing of Environment, 76,* 130-137

Blanc, L., & Dick, J.M. (2003). Errors in repeated measurements of soil water content in pots using a ThetaProbe. *Soil Use and Management, 19,* 87-88

Bosch, D.D., Lakshmi, V., Jackson, T.J., Choi, M., & Jacobs, J.M. (2006). Large scale measurements of soil moisture for validation of remotely sensed data: Georgia soil moisture experiment of 2003. *Journal of Hydrology, 323,* 120-137

Bourgeau-Chavez, L.L., Kasischke, E.S., Rutherford, M.D., & Bsp, M. (1999). Evaluation of ERS SAR Data for Prediction of Fire Danger in a Boreal Region. *International Journal of Wildland Fire, 9*, 183-194

Bourgeau-Chavez, L.L., Leblon, B., Charbonneau, F., & Buckley, J.R. (2013a). Assessment of polarimetric SAR data for discrimination between wet versus dry soil moisture conditions. *International Journal of Remote Sensing, 34*, 5709-5730

Bourgeau-Chavez, L.L., Leblon, B., Charbonneau, F., & Buckley, J.R. (2013b). Evaluation of polarimetric Radarsat-2 SAR data for development of soil moisture retrieval algorithms over a chronosequence of black spruce boreal forests. *Remote Sensing of Environment, 132*, 71-85

Brisco, B., & Brown, R.J. (1998). Agricultural Applications with Radar. In F.M. Henderson & A.J. Lewis (Eds.), *Principles and Applications of Imaging Radar, Manual of Remote Sensing*. Toronta: John Wiley & Sons, Inc.

Brisco, B., Pultz, T.J., Brown, R.J., Topp, G.C., Hares, M.A., & Zebchuk, W.D. (1992). Soil moisture measurement using portable dielectric probes and time domain reflectometry. *Water Resources Research, 28*, 1339-1346

Bryant, R., Moran, M.S., Thoma, D.P., Collins, C.D.H., Skirvin, S., Rahman, M., Slocum, K., Starks, P., Bosch, D., & Dugo, M.P.G. (2007). Measuring surface roughness height to parameterize radar backscatter models for retrieval of surface soil moisture. *Ieee Geoscience and Remote Sensing Letters, 4*, 137-141

Bryant, R., Thoma, D., Moran, S., Holifield, C., Goodrich, D., Keefer, T., Paige, G., Williams, D., & Skirvin, S. (2003). Evaluation of hyperspectral, infrared temperature and radar measurements for monitoring surface soil moisture. In, *Proceedings of the First Interagency Conference on Research in the Watersheds* (pp. 27-30)

Byron, N., & Shepherd, G. (2009). Indonesia and the 1997-98 El Niño: Fire problems and long term solutions. *ODI Natural Resource Perspectives, 28*, 1-14

Campbell, C., Vitt, D.H., Halsey, L.A., Campbell, I.D., Thormann,, M.N., & Bayley, S.E. (2000). Net primary production and standing biomass in northern continental wetlands. In (pp. 1-57). Northern Forestry Centre, Edmonton, Alberta. : Northern Forestry Centre

Campbell Scientific Inc. (2002). CS616 Water Content Reflectometer, User guide. In, *Logan, UT, USA*

Campbell Scientific Inc. (2003). CS616 and CS625 water content reflectometers instruction manual. In, *Campbell Scientific, Logan, UT*

Canadian Forest Service. (May 22, 2013). Canadian Forest Fire Weather Index (FWI) System. In *Canadian Wildland Fire Information System Background Information.* Retrieved September 26, 2013, from http://cwfis.cfs.nrcan.gc.ca/en_CA/background/summary/fwi.

Chin-Yuan, H., Fung, A.K., Nesti, G., Sieber, A.J., & Coppo, P. (1997). A further study of the IEM surface scattering model. *IEEE Transactions on Geoscience and Remote Sensing, 35*, 901-909

Cloude, S.R., & Pottier, E. (1996). A review of target decomposition theorems in radar polarimetry. *IEEE Transactions on Geoscience and Remote Sensing, 34*, 498-518

Damman, A.W.H. (1977). Geographical Changes in the Vegetation Pattern of Raised Bogs in the Bay of Fundy Region of Maine and New Brunswick. *Vegetatio, 35*, 137-151

Davidson, E.A., & Janssens, I.A. (2006). Temperature sensitivity of soil carbon decomposition and feedbacks to climate change. *Nature, 440*, 165-173

Davidson, M.W.J., Thuy Le, T., Mattia, F., Satalino, G., Manninen, T., & Borgeaud, M. (2000). On the characterization of agricultural soil roughness for radar remote sensing studies. *IEEE Transactions on Geoscience and Remote Sensing, 38*, 630-640

Delta-T Devices Ltd (1999). ThetaProbe Soil Moisture Sensor type ML2x User Manual. In, *Delta-T Devices* (p. 22). CB5 0EJ, Cambridge, UK: Delta-T Devices Ltd

Delta-T Devices Ltd (2013). ThetaProbe Soil Moisture Sensor type ML3 User Manual. In, *Delta-T Devices* (pp. 1-47). CB5 0EJ, Cambridge, UK: Delta-T Devices Ltd

Dise, N.B. (1993). Methane emission from Minnesota peatlands: Spatial and seasonal variability. *Global Biogeochemical Cycles, 7*, 123-142

Dobson, M.C., Ulaby, F.T., Hallikainen, M.T., & El-Rayes, M.A. (1985). Microwave Dielectric Behavior of Wet Soil-Part II: Dielectric Mixing Models. *Geoscience and Remote Sensing, IEEE Transactions on, GE-23*, 35-46

Dubois, P.C., van Zyl, J., & Engman, T. (1995). Measuring soil moisture with imaging radars. *Geoscience and Remote Sensing, IEEE Transactions on, 33*, 915-926

Engman, E.T., & Chauhan, N. (1995). Status of microwave soil moisture measurements with remote sensing. *Remote Sensing of Environment, 51*, 189-198

Environment Canada (2012). Canadian Climate Normals 1961-1990. In

Environment Canada (2013). Canadian Climate Normals 1971-2000. In

Escorihuela, M.J., De Rosnay, P., Kerr, Y.H., & Calvet, J.C. (2007). Influence of Bound-Water Relaxation Frequency on Soil Moisture Measurements. *Geoscience and Remote Sensing, IEEE Transactions on, 45*, 4067-4076

Flannigan, M., Stocks, B., Turetsky, M., & Wotton, M. (2009a). Impacts of climate change on fire activity and fire management in the circumboreal forest. *Global Change Biology, 15*, 549-560

Flannigan, M.D., Krawchuk, M.A., de Groot, W.J., Wotton, B.M., & Gowman, L.M. (2009b). Implications of changing climate for global wildland fire. *International Journal of Wildland Fire, 18*, 483-507

Frandsen, W.H. (1987). The influence of moisture and mineral soil on the combustion limits of smoldering forest duff. *Canadian Journal of Forest Research, 17*, 1540-1544

Fung, A.K. (1994). *Microwave Scattering and Emission Models and Their Applications*. Norwood, MA.: Artech House

Fung, A.K., Dawson, M.S., Chen, K.S., Hsu, A.Y., Engman, E.T., ONeill, P.O., & Wang, J. (1996). A modified IEM model for scattering from soil surfaces with application to soil moisture sensing. *Igarss '96 - 1996 International Geoscience and Remote Sensing Symposium: Remote Sensing for a Sustainable Future, Vols I - Iv*, 1297-1299

Fung, A.K., Li, Z., & Chen, K.S. (1992). Backscattering from a randomly rough dielectric surface. *Geoscience and Remote Sensing, IEEE Transactions on, 30*, 356-369

Gala, T.S., Aldred, D.A., Carlyle, S., & Creed, I.F. (2011). Topographically based spatially averaging of SAR data improves performance of soil moisture models. *Remote Sensing of Environment, 115*, 3507-3516

Gaskin, G.J., & Miller, J.D. (1996). Measurement of Soil Water Content Using a Simplified Impedance Measuring Technique. *Journal of Agricultural Engineering Research, 63*, 153-159

Gherboudj, I., Magagi, R., Berg, A.A., & Toth, B. (2011). Soil moisture retrieval over agricultural fields from multi-polarized and multi-angular RADARSAT-2 SAR data. *Remote Sensing of Environment, 115*, 33-43

Gorham, E. (1991). Northern Peatlands - Role in the Carbon-Cycle and Probable Responses to Climatic Warming. *Ecological Applications, 1*, 182-195

Hadden, R.M., Rein, G., & Belcher, C.M. (2013). Study of the competing chemical reactions in the initiation and spread of smouldering combustion in peat. *Proceedings of the Combustion Institute, 34*, 2547-2553

Hajnsek, I., Jagdhuber, T., Schcon, H., & Papathanassiou, K.P. (2009). Potential of Estimating Soil Moisture Under Vegetation Cover by Means of PolSAR. *IEEE Transactions on Geoscience and Remote Sensing, 47*, 442-454

Hansson, K., & Lundin, L.C. (2006). Water content reflectometer application to construction materials and its relation to time domain reflectometry. *Vadose Zone Journal, 5*, 459-468

Hare, F.K., & Thomas, M.K. (1979). *Climate Canada*. Toronto, Canada: J. Wiley & Sons Canada

Hogg, E.H. (1993). Decay Potential of Hummock and Hollow Sphagnum Peats at Different Depths in a Swedish Raised Bog. *Oikos, 66*, 269-278

Holden, J. (2005). Peatland hydrology and carbon release: why small-scale process matters. *Philosophical Transactions of the Royal Society A: Mathematical, Physical and Engineering Sciences, 363*, 2891-2913

Imhoff, M.L. (1995). Radar backscatter and biomass saturation: ramifications for global biomass inventory. *Geoscience and Remote Sensing, IEEE Transactions on, 33*, 511-518

Jackson, T.J. (1993). Measuring surface soil moisture using passive microwave remote sensing. *Hydrological processes, 7*, 139-152

Kaleita, A.L., Heitman, J.L., & Logsdon, S.D. (2005). Field calibration of the Theta Probe for Des Moines lobe soils. *Applied engineering in agriculture, 21*, 865-870

Kasischke, E.S., Bourgeau-Chavez, L.L., & Johnstone, J.F. (2007). Assessing spatial and temporal variations in surface soil moisture in fire-disturbed black spruce forests in Interior Alaska using spaceborne synthetic aperture radar imagery — Implications for post-fire tree recruitment. *Remote Sensing of Environment, 108*, 42-58

Kasischke, E.S., Morrissey, L., Way, J.B., French, N.H.F., Bourgeau-Chavez, L.L., Rignot, E., Steam, J.A., & Livingston, G.P. (1995). Monitoring seasonal variations in boreal ecosystems using multitemporal spaceborne SAR data. . *Canadian Journal of Remote Sensing, 21*, 96-109

Kellner, E., & Lundin, L.C. (2001). Calibration of time domain reflectometry for water content in peat soil. *Nordic Hydrology, 32*, 315-332

Koyama, C.N. (2012). Quantitative Estimation of Surface Soil Moisture in Agricultural Landscapes using Spaceborne Synthetic Aperture Radar Imaging at Different Frequencies and Polarizations In, *Mathematics and Natural Sciences* (p. 229). Bergisch Gladbach: Universität zu Köln

Koyama, C.N., Korres, W., Fiener, P., & Schneider, K. (2010). Variability of Surface Soil Moisture Observed from Multitemporal C-Band Synthetic Aperture Radar and Field Data. *Vadose Zone Journal, 9*, 1014-1014

Lakhankar, T., Krakauer, N., & Khanbilvardi, R. (2009). Applications of microwave remote sensing of soil moisture for agricultural applications. *International Journal of Terraspace Science and Engineering, 2*, 81-91

Larter, J.L. (2010). Remote sensing of a dynamic sub-arctic peatland reservoir using optical and synthetic aperture radar data. In, *Department of Environment and Geography* (pp. 1-212). Winnipeg, Manitoba, Canada: University of Manitoba

Lievens, H., & Verhoest, N.E.C. (2011). On the Retrieval of Soil Moisture in Wheat Fields From L-Band SAR Based on Water Cloud Modeling, the IEM, and Effective Roughness Parameters. *Ieee Geoscience and Remote Sensing Letters, 8*, 740-744

Lievens, H., Verhoest, N.E.C., De Keyser, E., Vernieuwe, H., Matgen, P., Alvarez-Mozos, J., & De Baets, B. (2011). Effective roughness modelling as a tool for soil moisture retrieval from C-and L-band SAR. *Hydrology and Earth System Sciences, 15*, 151-162

Lievens, H., Vernieuwe, H., Alvarez-Mozos, J., De Baets, B., & Verhoest, N.E.C. (2009). Error in Radar-Derived Soil Moisture due to Roughness Parameterization: An Analysis Based on Synthetical Surface Profiles. *Sensors (Basel, Switzerland), 9*, 1067-1093

Lin, L.I. (1989). A concordance correlation coefficient to evaluate reproducibility. *Biometrics, 45*, 255-268

Lin, L.I.K. (1992). Assay Validation Using the Concordance Correlation-Coefficient. *Biometrics, 48*, 599-604

Lu, D., Mausel, P., Brondízio, E., & Moran, E. (2004). Change detection techniques. *International Journal of Remote Sensing, 25*, 2365-2401

Luken, J.O. (1985). Zonation of Sphagnum Mosses - Interactions among Shoot Growth, Growth Form, and Water-Balance. *Bryologist, 88*, 374-379

MacDonald Dettwiler Associates Ltd (2009). Radarsat-2 product description. In (pp. 1-46)

MacDonald Dettwiler Associates Ltd (2011). Radarsat-2 Product Format Definition. In (pp. 1-83)

Mattia, F., Davidson, M.W.J., Le Toan, T., D'Haese, C.M.F., Verhoest, N.E.C., Gatti, A.M., & Borgeaud, M. (2003). A comparison between soil roughness statistics used in surface scattering models derived from mechanical and laser profilers. *IEEE Transactions on Geoscience and Remote Sensing, 41*, 1659-1671

Melloh, R., Mason, G., Berini, C., & Bailey, R. (2006). Spatial and temporal variation of 10-cm background soil moisture - art. no. 62171T. In, *Detection and Remediation Technologies for Mines and Minelike Targets XI, Pts 1 and 2* (pp. T2171-T2171)

Merzouki, A., McNairn, H., & Pacheco, A. (2010). Evaluation of the Dubois, Oh, and IEM radar backscatter models over agricultural fields using C-band RADARSAT-2 SAR image data. *Canadian Journal of Remote Sensing, 36*, S274-S286

Miller, J.R., White, H.P., Chen, J.M., Peddle, D.R., McDermid, G., Fournier, R.A., Shepherd, P., Rubinstein, I., Freemantle, J., Soffer, R., & LeDrew, E. (1997). Seasonal change in understory reflectance of boreal forests and influence on canopy vegetation indices. *Journal of Geophysical Research: Atmospheres, 102*, 29475-29482

Moore, P.D. (1989). The Ecology of Peat-Forming Processes - a Review. *International Journal of Coal Geology, 12*, 89-103

Moore, T.R., & Knowles, R. (1989). The Influence of Water-Table Levels on Methane and Carbon-Dioxide Emissions from Peatland Soils. *Canadian Journal of Soil Science, 69*, 33-38

Moran, M.S., Hymer, D.C., Qi, J., & Kerr, Y. (2002). Comparison of ERS-2 SAR and Landsat TM imagery for monitoring agricultural crop and soil conditions. *Remote Sensing of Environment, 79*, 243-252

Moran, S.M., Hymer, D.C., Qi, J., & Sano, E.E. (2000). Soil moisture evaluation using multi-temporal synthetic aperture radar (SAR) in semiarid rangeland. *Agricultural and Forest Meteorology, 105*, 69-80

Nagare, R.M., Schincariol, R.A., Quinton, W.L., & Hayashi, M. (2011). Laboratory calibration of time domain reflectometry to determine moisture content in undisturbed peat samples. *European Journal of Soil Science, 62*, 505-515

National Wetlands Working Group (1988). Wetlands of Canada. . In, *Ecological Land Classification Series*: Sustainable Development Branch, Environment Canada

Natural Resources Canada (2013). Natural Resources Canada Topographic Maps - Canvec. In

Nemali, K.S., Montesano, F., Dove, S.K., & van Iersel, M.W. (2007). Calibration and performance of moisture sensors in soilless substrates: ECH2O and Theta probes. *Scientia Horticulturae, 112*, 227-234

Niederleitner, J. (1976). Detecting holdover fires with the AGA Thermovision 750 infrared scanner. In (pp. 1-43): Northern Forest Research Centre

Nungesser, M.K. (2003). Modelling microtopography in boreal peatlands: hummocks and hollows. *Ecological Modelling, 165*, 175-207

Oh, Y. (2004). Quantitative retrieval of soil moisture content and surface roughness from multipolarized radar observations of bare soil surfaces. *IEEE Transactions on Geoscience and Remote Sensing, 42*, 596-601

Ohlemiller, T. (2002). Smoldering combustion. *SFPE Handbook of Fire Protection Engineering* (pp. 200-210): Center for Fire Research

Overduin, P.P., Yoshikawa, K., Kane, D.L., & Harden, J.W. (2005). Comparing electronic probes for volumetric water content of low-density feathermoss. *Sensor Review, 25*, 215-221

Paloscia, S., Pampaloni, P., Pettinato, S., & Santi, E. (2008). A Comparison of Algorithms for Retrieving Soil Moisture from ENVISAT/ASAR Images. *Geoscience and Remote Sensing, IEEE Transactions on, 46*, 3274-3284

Pohl, C., & Van Genderen, J.L. (1998). Review article Multisensor image fusion in remote sensing: Concepts, methods and applications. *International Journal of Remote Sensing, 19*, 823-854

Rahman, M.M., Moran, M.S., Thoma, D.P., Bryant, R., Sano, E.E., Holifield Collins, C.D., Skirvin, S., Kershner, C., & Orr, B.J. (2007). A derivation of roughness correlation length for parameterizing radar backscatter models. *International Journal of Remote Sensing, 28*, 3995-4012

Ramsey, E.W. (1995). Radar remote sensing of wetlands. *Remote Sensing Change Detection: Environmental Monitoring Methods and Applications* (pp. 211-243): CRC press

Rappold, A.G., Stone, S.L., Cascio, W.E., Neas, L.M., Kilaru, V.J., Carraway, M.S., Szykman, J.J., Ising, A., Cleve, W.E., Meredith, J.T., Vaughan-Batten, H., Deyneka, L., & Devlin, R.B. (2011). Peat Bog Wildfire Smoke Exposure in Rural North Carolina Is Associated with Cardiopulmonary Emergency Department Visits Assessed through Syndromic Surveillance. *Environmental health perspectives, 119*, 1415-1420

Rein, G. (2009). Smouldering combustion phenomena in science and technology. *International Review of Chemical Engineering, 1*, 3-18

Robinson, D.A., Gardner, C.M.K., & Cooper, J.D. (1999). Measurement of relative permittivity in sandy soils using TDR, capacitance and theta probes: comparison,

including the effects of bulk soil electrical conductivity. *Journal of Hydrology, 223*, 198-211

Rydin, H. (1986). Competition and Niche Separation in Sphagnum. *Canadian Journal of Botany-Revue Canadienne De Botanique, 64*, 1817-1824

Rydin, H. (1993). Interspecific Competition between Sphagnum Mosses on a Raised Bog. *Oikos, 66*, 413-423

Rydin, H., Gunnarsson, U., & Sundberg, S. (2006). The Role of Sphagnum in Peatland Development and Persistence. In R.K. Wieder & D. Vitt (Eds.), *Boreal Peatland Ecosystems* (pp. 47-65): Springer Berlin Heidelberg

Sano, E.E., Huete, A.R., Troufleau, D., Moran, M.S., & Vidal, A. (1998). Relation between ERS-1 synthetic aperture radar data and measurements of surface roughness and moisture content of rocky soils in a semiarid rangeland. *Water Resources Research, 34*, 1491-1498

Sass, G.Z., & Creed, I.F. (2008). Characterizing hydrodynamics on boreal landscapes using archived synthetic aperture radar imagery. *Hydrological Processes, 22*, 1687-1699

Schimel, D., & Baker, D. (2002). Carbon cycle: the wildfire factor. *Nature, 420*, 29-30

Schmugge, T., Gloersen, P., Wilheit, T., & Geiger, F. (1974). Remote Sensing of Soil Moisture With Microwave Radiometers. *J. Geophys. Res., 79*, 317-323

Schmugge, T.J., Kustas, W.P., Ritchie, J.C., Jackson, T.J., & Rango, A. (2002). Remote sensing in hydrology. *Advances in Water Resources, 25*, 1367-1385

Shepard, M.K., & Campbell, B.A. (1999). Radar scattering from a self-affine fractal surface: Near-nadir regime. *Icarus, 141*, 156-171

Sikdar, M., MacIntosh, S., Cumming, I., & Brisco, B. (2005). Incorporating a vegetation index into a soil moisture retrieval model - results from convair-580 SAR data.

*Proceedings. 2005 IEEE International Geoscience and Remote Sensing Symposium, 2005. IGARSS '05., 1*, 383-386

Sonnentag, O., Chen, J.M., Roberts, D.A., Talbot, J., Halligan, K.Q., & Govind, A. (2007). Mapping tree and shrub leaf area indices in an ombrotrophic peatland through multiple endmember spectral unmixing. *Remote Sensing of Environment, 109*, 342-360

Soria-Ruiz, J., McNairm, H., Fernandez-Ordonez, Y., & Bugden-Storie, J. (2007). Corn monitoring and crop yield using optical and RADARSAT-2 images. In, *Geoscience and Remote Sensing Symposium, 2007. IGARSS 2007. IEEE International* (pp. 3655-3658)

Tansey, K.J., & Millington, A.C. (1998). Remote sensing of desert surface processes and properties using multi-temporal radar imagery. In, *Geoscience and Remote Sensing Symposium Proceedings, 1998. IGARSS '98. 1998 IEEE International* (pp. 1348-1350 vol.1343)

Thoma, D., Moran, M., Bryant, R., Collins, C.H., Rahman, M., & Skirvin, S. (2004). Comparison of two methods for extracting surface soil moisture from C-band radar imagery. In, *Geoscience and Remote Sensing Symposium, 2004. IGARSS '04. Proceedings. 2004 IEEE International* (pp. 827-830)

Thompson, D.K., & Waddington, J.M. (2013). Wildfire effects on vadose zone hydrology in forested boreal peatland microforms. *Journal of Hydrology, 486*, 48-56

Topp, G.C., Davis, J.L., & Annan, A.P. (1980). Electromagnetic determination of soil water content: Measurements in coaxial transmission lines. *Water Resour. Res., 16*, 574-582

Touzi, R., Boerner, W.M., Lee, J.S., & Lueneburg, E. (2004). A review of polarimetry in the context of synthetic aperture radar: concepts and information extraction. *Canadian Journal of Remote Sensing, 30*, 380-407

Turetsky, M., Wieder, K., Halsey, L., & Vitt, D. (2002). Current disturbance and the diminishing peatland carbon sink. *Geophysical Research Letters, 29*, 1-4

Turetsky, M.R., Amiro, B.D., Bosch, E., & Bhatti, J.S. (2004). Historical burn area in western Canadian peatlands and its relationship to fire weather indices. *Global Biogeochemical Cycles, 18*, 1-9

Turetsky, M.R., & Louis, V.L.S. (2006). Disturbance in boreal peatlands. In R.K. Wieder & D.H. Vitt (Eds.), *Boreal Peatland Ecosystems* (pp. 359-379): Springer

Turunen, J., Tomppo, E., Tolonen, K., & Reinikainen, A. (2002). Estimating carbon accumulation rates of undrained mires in Finland–application to boreal and subarctic regions. *The Holocene, 12*, 69-80

Ulaby, F.T., Dubois, P.C., & van Zyl, J. (1996). Radar mapping of surface soil moisture. *Journal of Hydrology, 184*, 57-84

Ulaby, F.T., Moore, R.K., & Fung, A.K. (1981). Fundamentals and Radiometry. In D.S. Simonett (Ed.), *Microwave remote sensing:Active and Passive* (p. 456). Reading, Massachusetts: Addison-Wesley

Ulaby, F.T., Moore, R.K., & Fung, A.K. (1986). From Theory to Applications. *Microwave Remote Sensing, Active and Passive*. Norwood, MA, USA: Artech House

Van Wagner, C. (1987). Development and structure of the Canadian forest fire weather index system. In, *Forest Technical Report* Ottawa, Canada: Canadian Forest Service

Verhoest, N.E.C., Lievens, H., Wagner, W., Alvarez-Mozos, J., Moran, M.S., & Mattia, F. (2008). On the soil roughness parameterization problem in soil moisture retrieval of bare surfaces from synthetic aperture radar. *Sensors, 8*, 4213-4248

Vitt, D.H., Bayley, S.E., & Jin, T.-L. (1995). Seasonal variation in water chemistry over a bog-rich fen gradient in Continental Western Canada. *Canadian Journal of Fisheries and Aquatic Sciences, 52*, 587-606

Vitt, D.H., Halsey, L.A., & Zoltai, S.C. (1994). The Bog Landforms of Continental Western Canada in Relation to Climate and Permafrost Patterns. *Arctic and Alpine Research, 26*, 1-13

Vitt, D.H., & Slack, N.G. (1975). An analysis of the vegetation of Sphagnum-dominated kettle-hole bogs in relation to environmental gradients. *Canadian Journal of Botany, 53*, 332-359

Waddington, J.M., Thompson, D.K., Wotton, M., Quinton, W.L., Flannigan, M.D., Benscoter, B.W., Baisley, S.A., & Turetsky, M.R. (2012). Examining the utility of the Canadian Forest Fire Weather Index System in boreal peatlands. *Canadian Journal of Forest Research, 42*, 47-58

Wang, C., & Qi, J. (2000). Soil moisture extraction in sparse vegetated area using SAR and TM data. In, *Geoscience and Remote Sensing Symposium, 2000. Proceedings. IGARSS 2000. IEEE 2000 International* (pp. 1265-1267 vol.1263)

Wang, C., Qi, J., Moran, S., & Marsett, R. (2004). Soil moisture estimation in a semiarid rangeland using ERS-2 and TM imagery. *Remote Sensing of Environment, 90*, 178-189

Wang, Y., Kasischke, E.S., Bourgeau-Chavez, L.L., O'Neill, K.P., & French, N.H.F. (2000). Assessing the influence of vegetation cover on soil-moisture signatures in fire-disturbed boreal forests in interior Alaska: Modelled results. *International Journal of Remote Sensing, 21*, 689-708

Warner, T.A. (2010). Remote-Sensing Analysis: From Project Design to Implementation. In J.D. Bossler, J.B. Campbell, R.B. McMaster & C. Rizos (Eds.), *Manual of Geospatial Science and Technology* (pp. 301-318): CRC Press

Watts, A., & Kobziar, L. (2013). Smoldering combustion and ground fires: ecological effects and multi-scale significance. *Fire Ecology, 9*, 124-132

Watts, A.C., & Kobziar, L.N. (2012). Smoldering Combustion in Organic Soils: Peat and Muck Fires in the Southeastern US. In, *SFE Research Synthesis* (pp. 1-5)

Wein, R.W., & Bliss, L.C. (1973). Changes in Arctic Eriophorum Tussock Communities Following Fire. *Ecology, 54*, 845-852

Wickel, A.J., Jackson, T.J., & Wood, E.F. (2001). Multitemporal monitoring of soil moisture with RADARSAT SAR during the 1997 Southern Great Plains hydrology experiment. *International Journal of Remote Sensing, 22*, 1571-1583

Wohlfarth, C. (2005). Permittivity (dielectric constant) of liquids. *CRC Handbook of physics and chemistry, 85th ed. CRC Press, Boca Raton, FL*

Yoshikawa, K., Overduin, P.P., & Harden, J.W. (2004). Moisture content measurements of moss (Sphagnum spp.) using commercial sensors. *Permafrost and Periglacial Processes, 15*, 309-318

Zoltai, S.C., Morrissey, L.A., Livingston, G.P., & de Groot, W.J. (1998). Effects of fire on carbon cycling in North American boreal peatlands. *Environmental Reviews, 6*, 13-24

# Appendix

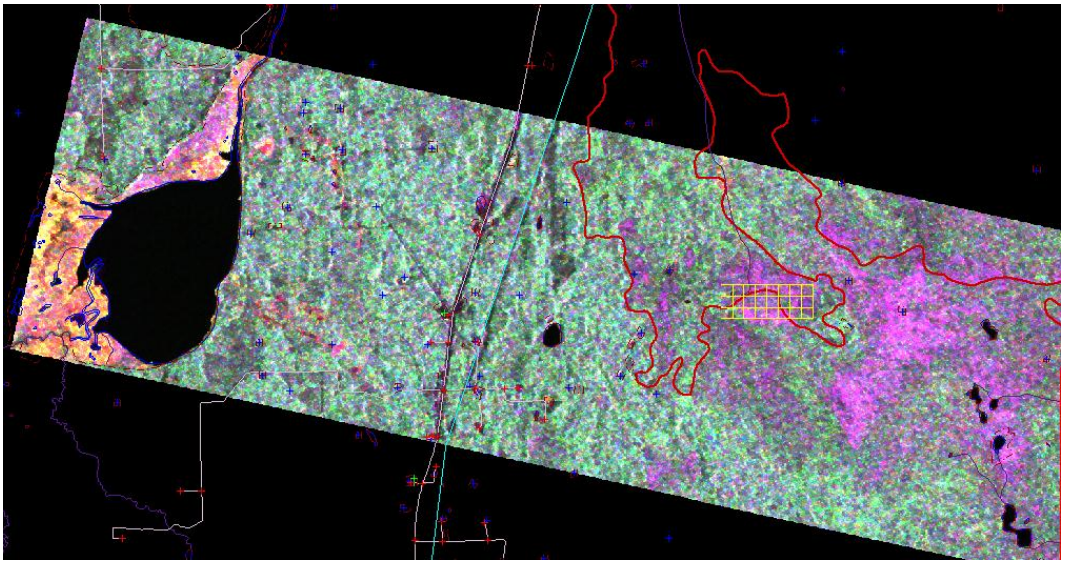

Figure A- 1. Radarsat-2 polarization color composited image, with HH coded as red, HV as green and VV as blue for 0710.

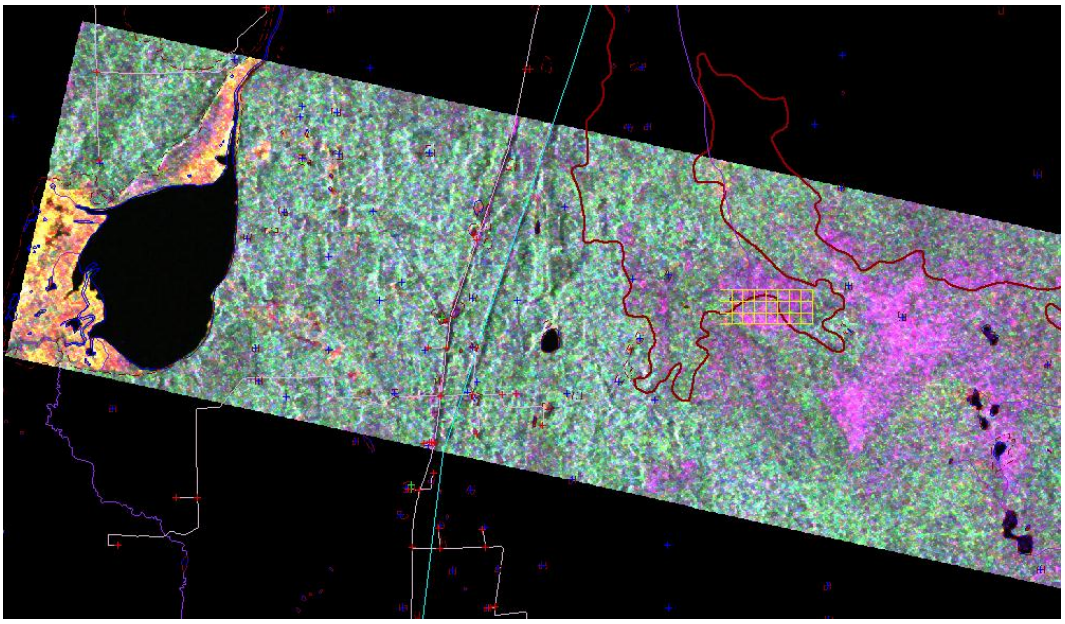

Figure A- 2. Radarsat-2 polarization color composited image, with HH coded as red, HV as green and VV as blue for 0803.

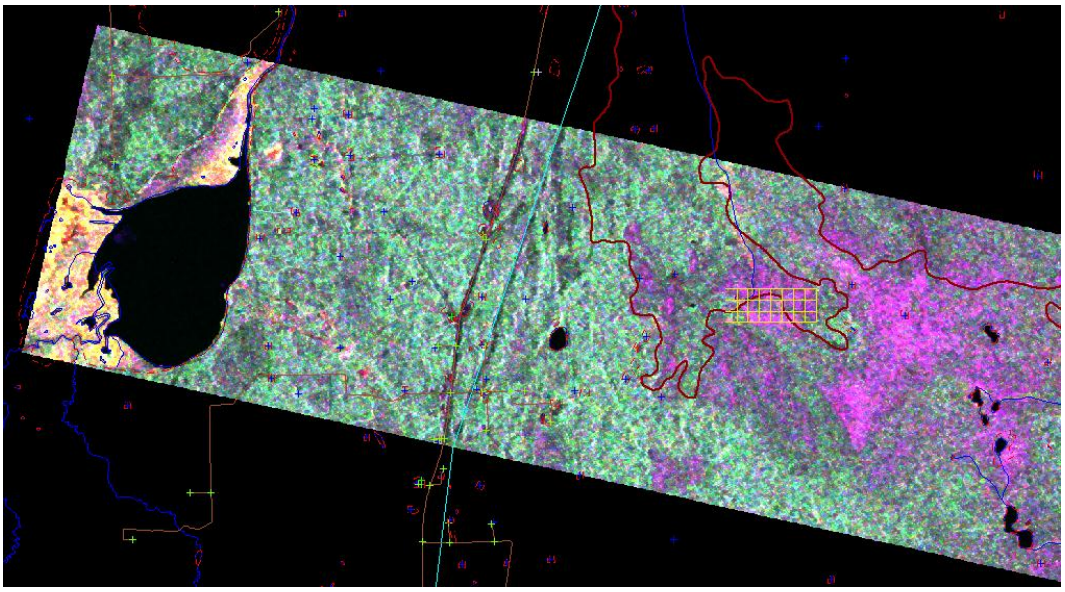

Figure A- 3. Radarsat-2 polarization color composited image, with HH coded as red, HV as green and VV as blue for 0827.

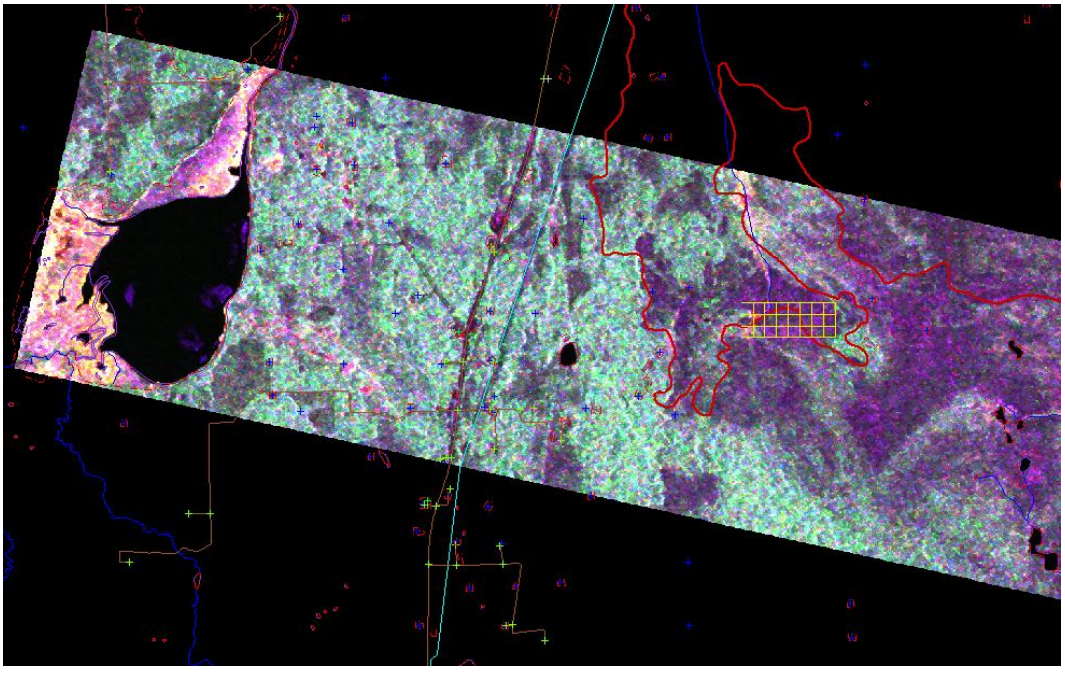

Figure A- 4. Radarsat-2 polarization color composited image, with HH coded as red, HV as green and VV as blue for 0920.